DYNAMIC MODELING OF SINGLE-PHASE INDUCTION MOTOR LOADS

by

Danyal Mohammadi

A thesis

submitted in partial fulfillment

of the requirements for the degree of

Master of Science in Electrical Engineering

Boise State University

August 2012

BOISE STATE UNIVERSITY GRADUATE COLLEGE

DEFENSE COMMITTEE AND FINAL READING APPROVALS

of the thesis submitted by

Danyal Mohammadi

Thesis Title: Dynamic Modeling of Single-Phase Induction Motor Loads

Date of Final Oral Examination: 23 August 2012

The following individuals read and discussed the thesis submitted by student Danyal Mohammadi, and they evaluated his presentation and response to questions during the final oral examination. They found that the student passed the final oral examination.

Said Ahmed-Zaid, Ph.D.	Chair, Supervisory Committee
John Chiasson, Ph.D.	Member, Supervisory Committee
Jim Browning, Ph.D.	Member, Supervisory Committee

The final reading approval of the thesis was granted by Said Ahmed-Zaid, Ph.D., Chair of the Supervisory Committee. The thesis was approved for the Graduate College by John R. Pelton, Ph.D., Dean of the Graduate College.

To my Parents

ACKNOWLEDGMENTS

I would like to thank my advisor, Professor Said Ahmed-Zaid, for giving me the opportunity to pursue this research. His guidance and encouragement have been invaluable. I would also like to thank all the professors at Boise State University who have taught me so much during my graduate career. In particular, I am grateful for taking courses from Professor John Chiasson and Professor Jim Browning who were also members of my supervisory committee.

Finally, I would like to acknowledge the support of the Boise State University Electrical and Computer Engineering department with a graduate assistantship during the 2011-2012 academic year.

ABSTRACT

Single-phase induction machines are found in various appliances such as refrigerators, washing machines, driers, air conditioners, and fans. Large concentrations of single-phase induction motor loads such as air conditioners and other motor-compressor loads can adversely impact the dynamic performance of a power system. An understanding of the dynamics of this type of induction machine is needed to improve the current state of the art in running power system dynamic studies.

In this thesis, a novel approach of modeling an exact fourth-order model of a single-phase induction machine is developed that gives credence to the well-known double revolving-field theory. Using a standard averaging technique, an augmented seventh-order dynamic model is derived using forward- and backward-rotating components. The double-frequency terms causing torque and speed pulsations in the original model can be recovered as a byproduct of the theory. It is proved that two three-phase induction machines with their stator windings connected in series but with opposite phase sequence have the same dynamical behavior as the averaged single-phase induction machine model. The dynamic and steady-state performances of the single-phase machine are investigated using the new augmented model and compared with the exact model.

TABLE OF CONTENTS

LIST OF TABLES

LIST OF FIGURES

LIST OF SYMBOLS

R_s	Stator Winding Resistance
R_r	Rotor Resistance
ω_s	Electrical Excitation Frequency
ω_m	Mechanical Shaft Speed
ω	Electrical Shaft Speed
$X_{\ell s}$	Stator Leakage Reactance
$X_{\ell r}$	Rotor Leakage Reactance
X_{ms}	Mutual Reactance
$L_{\ell s}$	Stator Leakage Inductance
$L_{\ell r}$	Rotor Leakage Inductance
L_{ms}	Stator Magnetizing Inductance
J	Moment of Inertia

CHAPTER 1

INTRODUCTION

1.1 Research Motivation

The adequate modeling of all power system configurations and components is critical to the determination of accurate power system stability results [1]. Power system loads are modeled with both static and dynamic load models. Static load models are represented by constant power, constant current, and constant impedance models, or some combination of these three types. Induction motor loads are usually separated using a first-order speed model for small-type motors and by a third-order model for large-type induction motors.

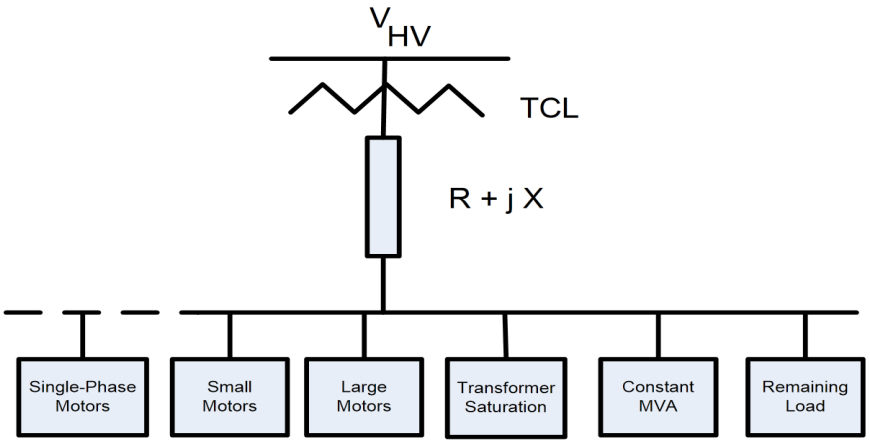

Figure 1.1: Complex Load Model

Modeling the diverse characteristics of a system load gives a more detailed and accurate system response to voltage and frequency changes [2]. Load types are decomposed into groups of similar components, as shown in Figure 1.1, where V_{HV} and TCL respectively stand for the high-voltage bus and a tap-changing-under-load transformer, and $R + jX$ represents a subtransmission line.

Electrical motors consume about 70% of the electrical energy produced in the United States. Mostly static models are used to represent induction machines which accurately model the real power consumption but ignore the reactive power. Therefore, dynamic models must be used [3]. With stability and voltage problems on the rise, it has become necessary to include the dynamic characteristics of single-phase induction machines in the dynamic simulation of power systems.

Single-phase induction machines are commonly found in many household appliances. Most single-phase induction machines are small and built in the fractional horse-power range. Since single-phase induction motor loads make up a significant portion of some power systems, it is important to develop accurate models for use in stability studies.

The dynamic model of the single-phase induction machine currently used exhibits small double-frequency pulsations superimposed on a steady-state speed. These double-frequency oscillations exist at an operating point and make it difficult to assess its small-signal stability. Therefore, it is important to develop an equivalent model with no oscillations in steady state.

This thesis proposes a new approach to the modeling of a single-phase induction machine by combining averaging and double revolving-field theories. Applying this approach to the well-known model of single-phase induction machine yields a new model where double-frequency terms can be averaged over time yielding an

autonomous system with a static equilibrium point. This new averaged model can be linearized and its eigenvalues can be used to assess the stability of an operating point.

1.2 Literature Review

How a single-phase induction motor functions has been a topic of discussion for many years. Even though these theories describe the motor performance well, no adequate analysis has shown how the various theories compare on the shortcomings [4].

Several theories such as the cross-field theory, the double revolving-field theory, and dynamic phasors [5] have been proposed to explain the behavior of single-phase induction machines. In the following sections, the fundamentals of double revolving-field theory and dynamic phasors will be reviewed.

1.2.1 Double Revolving-Field Theory

The double-field revolving theory was proposed to explain why there is zero shaft torque at standstill and yet torque once rotated. This theory is based on resolving an alternating quantity into two components rotating in opposite directions with each one of them having half the maximum amplitude of the alternating quantity.

Two conditions will be discussed for a single-phase induction machine using the double revolving-field theory: when the rotor is standstill and when the rotor is running. When the rotor is at standstill, the torque developed by the forward- and backward-rotating components is zero.

When the rotor is spinning, as speed increases, the forward flux increases the driving torque while the backward flux decreases and reduces the opposing torque.

The motor quickly accelerates to a final speed near synchronous speed. In the single-phase induction machine shown in Figure 1.2, the stator winding produces a stationary alternating magnetic field $\vec{B}_s$ (OP), which can be decomposed into a forward-rotating field $\bar{B}_f$ (with magnitude OR) and a backward-rotating field $\vec{B}_b$ (with magnitude OR) such that OP=2OR.

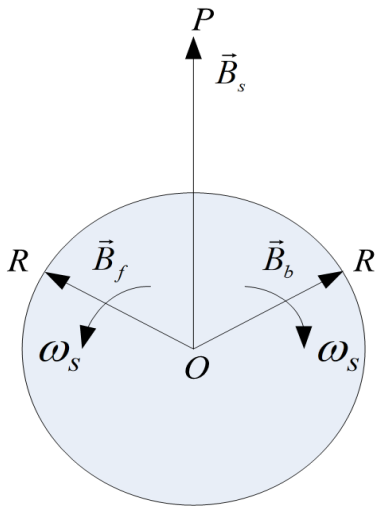

Figure 1.2: Forward and Backward Components of a Stationary Sinusoidal Magnetic Field

Based on the double revolving-field theory, the forward and backward components of the field are rotating in opposite directions and the machine rotates in the forward direction. Therefore, these components interact with each other at twice the electrical frequency resulting in double-frequency speed pulsations as shown in Figure 1.3.

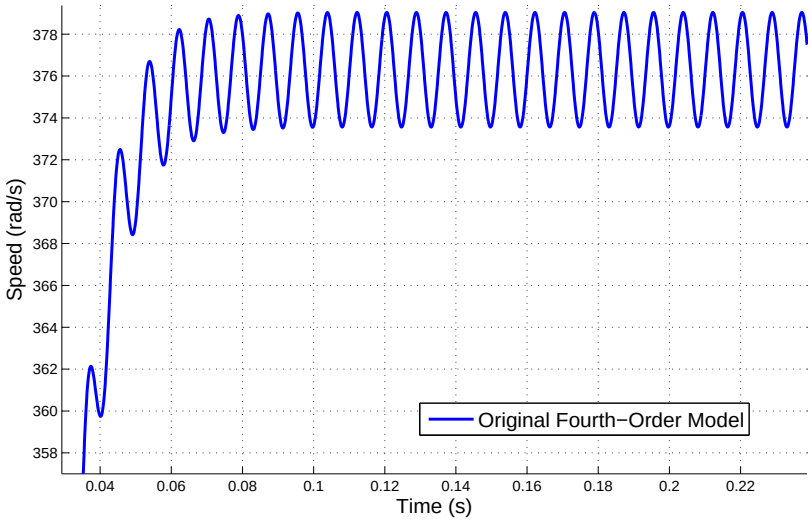

Figure 1.3: Speed Oscillations

As these two components rotate, they cut the rotor conductors inducing currents in the short-circuited rotor windings. As shown in Figure 1.4, the torque resulting from the forward-rotating current components is positive while the torque due to the backward-rotating components is negative. By symmetry, the net produced torque is zero at standstill [6] where ω is the machine speed and s is the slip defined as

$$s = \frac{\omega_s - \omega}{\omega_s}. \tag{1.1}$$

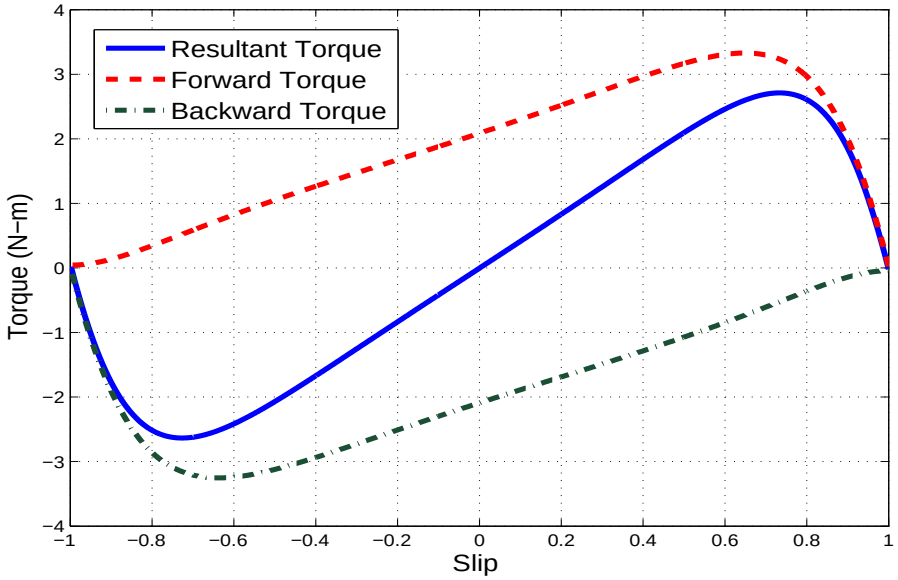

Figure 1.4: Forward and Backward Torque

1.2.2 Dynamic Phasors

The main idea behind dynamic phasors is to approximate a possibly complex time domain waveform $x(\tau)$ in the interval $\tau \in (t-T, t]$ with a Fourier series representation of the form

$$x(\tau) \quad = \quad \sum_{k=-\infty}^{\infty} X^k(t) e^{jk\omega_b \tau} \tag{1.2}$$

where

$$X^k(t) \quad = \quad \frac{1}{T} \int_{t-T}^{t} x(\tau) e^{-jk\omega_b \tau} d\tau \quad = \quad < x >_k (t) \tag{1.3}$$

and $\omega_b = 2\pi/T$ and $X^k(t)$ is the k-th time-varying Fourier coefficient in complex form, also called a dynamic phasor, and k is the set of selected Fourier coefficients,

which provide a good approximation of the original waveform (e.g., k = 0, 1, 2) [5].

In this approach, each of the state variables is expressed in terms of a Fourier series with time-varying coefficients, and at steady state the dynamic phasors X^k become constant [7]. This approach can average the state variable oscillations by retaining some of the harmonics that are often based on physical intuition [5]. Simulating the single-phase induction machine by this approach yields the green upper envelope and red lower envelope of the speed response as shown in Figure 1.5.

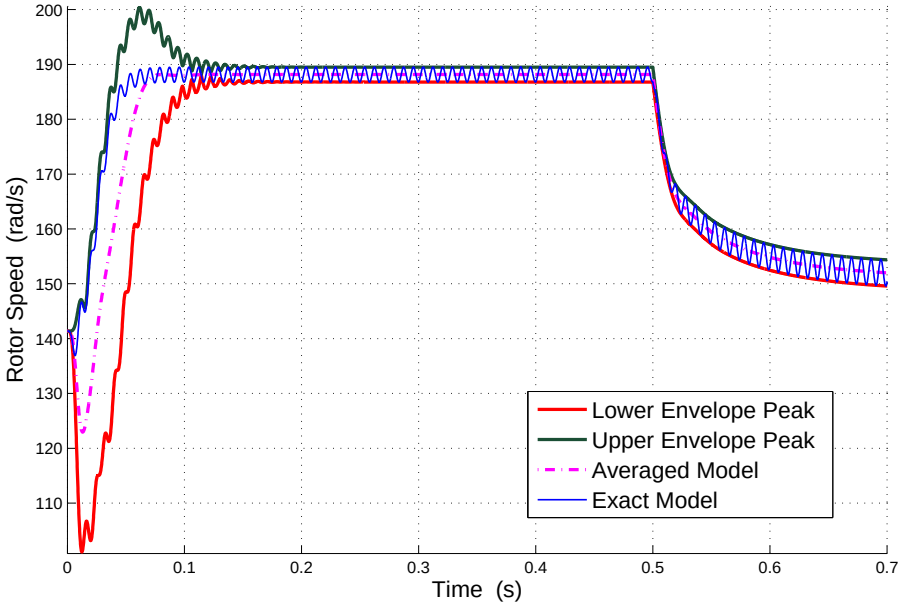

Figure 1.5: Simulation of the Single-Phase Induction Machine Using Dynamic Phasors

The authors in reference [5] object to the traditional derivation of the equivalent circuit of a single-phase induction motor that relies upon the principle of superposition by decomposing a quantity such as magnetic field into the sum of two separate components. Their argument is justified by the fact that the principle of superposition cannot be applied to a nonlinear system model.

In this thesis, we will reconcile the double revolving-field theory and the use of dynamic phasors by showing that the principle of superposition applies to the torque equation of an averaged augmented model that will be derived in Chapter 2.

1.3 Thesis Organization

In Chapter 2, we develop a novel approach of modeling a fourth-order model of a single-phase induction machine based on an exact transformation of the original electrical variables into well-defined forward and backward components yielding an augmented seventh-order model that produces an identical dynamic behavior of the single-phase induction machine under loading transients.

This novel approach is based on standard averaging theory applied to find a seventh-order averaged model of a single-phase induction machine in which there are no speed pulsations in steady state.

In Chapter 3, a new model is obtained for two three-phase induction machines connected in series but with opposite stator phase sequence. The derived seventh-order model represents both machines coupled on the same shaft and is dynamically equivalent to the augmented averaged model of a single-phase induction machine with forward and backward components. These two models clarify the objection in [5] and yield a seventh-order dynamic model suitable for power system stability studies.

In Chapter 4, several applications are used to validate the developed models. An eigenvalue analysis is used to confirm the speed or slip at which maximum pull-out torque occurs. A participation factor analysis shows that the shaft speed is the state variable associated with a dominant real eigenvalue. This analysis is used to derive a first-order speed model of the machine in conjunction with a quasi-steady-state

circuit describing the stator and rotor transients. Finally, a transient stability analysis gives comparable values for the critical torque applied from a no-load condition to various models of a single-phase induction machine. Chapter 5 summarizes the main conclusions derived in this work and makes some recommendations for future work.

CHAPTER 2

MODELING OF SINGLE-PHASE INDUCTION MACHINES

In this chapter, the modeling of a single-phase induction machine is developed for the type commonly referred to as a squirrel-cage motor. In this rotating machine, the rotor consists of a number of conducting bars short-circuited by conducting rings at both ends of the squirrel cage.

2.1 Model in Rotor ab-Coordinates

A single-phase induction machine has one distributed stator winding and two equivalent rotor windings modeling the squirrel cage. One of the main characteristics of a single-phase induction machine is that the machine does not produce a torque at standstill. As with other types of single-phase machines, it needs an auxiliary winding to produce a non-zero starting torque at standstill that will cause the shaft to accelerate to near synchronous mechanical speed at no load. A fifth-order differential model of the single-phase induction motor in rotor (a,b) coordinates is given by

$$v_{sa} = R_s i_{sa} + \frac{d\lambda_{sa}}{dt} \tag{2.1}$$

$$0 = R_r i_{ra} + \frac{d\lambda_{ra}}{dt} \tag{2.2}$$

$$0 = R_r i_{rb} + \frac{d\lambda_{rb}}{dt} \tag{2.3}$$

$$\frac{d\theta}{dt} = \omega \tag{2.4}$$

$$\frac{J}{p/2}\frac{d\omega}{dt} = T_e - T_m \tag{2.5}$$

where the label "s" denotes the stator winding, and the labels "ra" and "rb" denote the rotor phase-a and phase-b windings. The variable λ_s is the stator flux and λ_{ra} and λ_{rb} are, respectively, the rotor fluxes of phases a and b. The electrical angle between the stator winding and the phase-a rotor winding is defined as θ. The electromagnetic torque and the mechanical load torque are defined, respectively, as T_e and T_m.

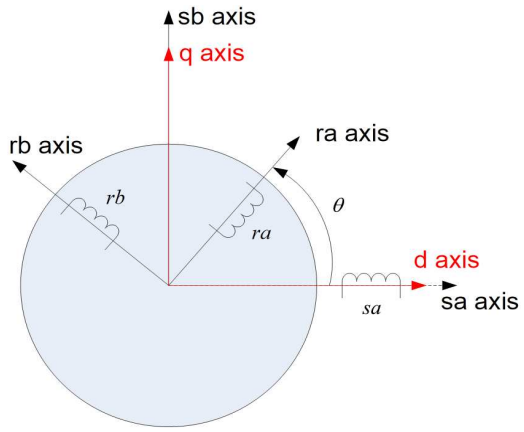

Figure 2.1: Stator and Rotor Windings in ab Coordinates

The auxiliary winding equation is not included in this model because it is open-circuited by a centrifugal switch when the shaft speed reaches 75 to 80% of its rated speed. The flux-current relationships are given by

$$\begin{bmatrix} \lambda_{sa} \\ \lambda_{ra} \\ \lambda_{rb} \end{bmatrix} = \begin{bmatrix} L_{\ell s} + L_{ms} & L_{ms}\cos\theta & -L_{ms}\sin\theta \\ L_{ms}\cos\theta & L_{\ell r} + L_{ms} & 0 \\ -L_{ms}\sin\theta & 0 & L_{\ell r} + L_{ms} \end{bmatrix} \begin{bmatrix} i_{sa} \\ i_{ra} \\ i_{rb} \end{bmatrix} \tag{2.6}$$

where $L_{\ell s}$ and $L_{\ell r}$ are the stator and rotor leakage inductances, respectively, and L_{ms} is the stator magnetizing inductance. It is assumed that the rotor variables have been referred to the stator side through the use of an effective stator-to-rotor turns ratio. Assuming an electrically-linear machine, the magnetic co-energy is equal to

$$W'_m = \frac{1}{2}\lambda_{sa} i_{sb} + \frac{1}{2}\lambda_{ra} i_{ra} + \frac{1}{2}\lambda_{rb} i_{rb}. \tag{2.7}$$

Using Equation (2.6), the co-energy is expressed in terms of inductances as

$$\begin{aligned} W'_m &= \frac{1}{2}\left(L_{\ell s} + L_{ms}\right) i_{sa}^2 + \frac{1}{2}\left(L_{\ell r} + L_{ms}\right)\left(i_{ra}^2 + i_{rb}^2\right) \\ &\quad + L_{ms} i_{sa}\left(i_{ra}\cos\theta - i_{rb}\sin\theta\right). \end{aligned} \tag{2.8}$$

The electromagnetic torque developed by the machine is then given by

$$T_e = \frac{\partial W'_m}{\partial \theta_m} = \left(\frac{p}{2}\right)\frac{\partial W'_m}{\partial \theta} \tag{2.9}$$

where θ_m denotes the mechanical angle of rotation related to the electrical angle θ by

$$\theta = \left(\frac{p}{2}\right)\theta_m \tag{2.10}$$

where p denotes the number of poles per phase. Taking the derivative of Equation (2.8) with respect to θ, the developed electromagnetic torque is equal to

$$T_e = -\left(\frac{p}{2}\right) L_{ms} i_{sa} \left(i_{ra} \sin\theta + i_{rb} \cos\theta\right). \tag{2.11}$$

2.2 Model in Rotor dq-Coordinates

The rotor variables of a single-phase induction machine in ab-coordinates are now transformed to dq coordinates as shown in Figure 2.2, where the fictitious dq windings appear stationary with respect to the stator.

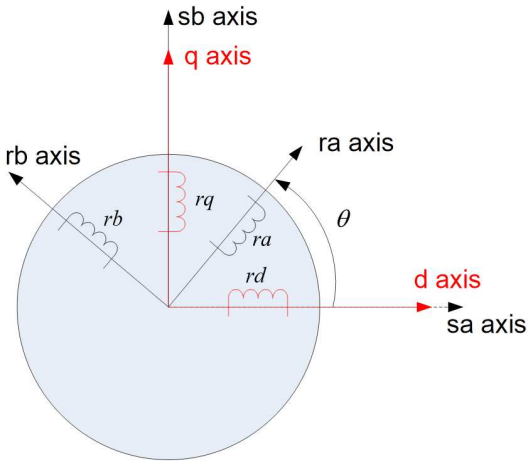

Figure 2.2: Projecting Rotor Windings to dq Coordinate

The new dq reference frame is stationary with respect to the stator sa-axis. In this case, the d-axis is aligned with the sa-axis, whereas in another case the q-axis may be aligned with the sa-axis [8]. To clarify this notation, the model of a single-phase induction machine will be obtained in both ways. First, the model will be obtained with the d-axis aligned with the sa-axis. Currents are given by

$$\begin{bmatrix} i_{rd} \\ i_{rq} \end{bmatrix} = \begin{bmatrix} \cos\theta & -\sin\theta \\ \sin\theta & \cos\theta \end{bmatrix} \begin{bmatrix} i_{ra} \\ i_{rb} \end{bmatrix} \tag{2.12}$$

and fluxes by

$$\begin{bmatrix} \psi_{rd} \\ \psi_{rq} \end{bmatrix} = \begin{bmatrix} \cos\theta & -\sin\theta \\ \sin\theta & \cos\theta \end{bmatrix} \begin{bmatrix} \psi_{ra} \\ \psi_{rb} \end{bmatrix}. \tag{2.13}$$

The inverse transformations are given by

$$\begin{bmatrix} i_{ra} \\ i_{rb} \end{bmatrix} = \begin{bmatrix} \cos\theta & \sin\theta \\ -\sin\theta & \cos\theta \end{bmatrix} \begin{bmatrix} i_{rd} \\ i_{rq} \end{bmatrix} \tag{2.14}$$

and

$$\begin{bmatrix} \psi_{ra} \\ \psi_{rb} \end{bmatrix} = \begin{bmatrix} \cos\theta & \sin\theta \\ -\sin\theta & \cos\theta \end{bmatrix} \begin{bmatrix} \psi_{rd} \\ \psi_{rq} \end{bmatrix}. \tag{2.15}$$

Using Equations (2.12) through (2.15), a fourth-order model is obtained in dq-coordinates as

$$v_{sd} = R_s i_{sd} + \frac{d\lambda_{sd}}{dt} \tag{2.16}$$

$$0 = R_r i_{rd} + \frac{d\lambda_{rd}}{dt} + \omega\lambda_{rq} \tag{2.17}$$

$$0 = R_r i_{rq} + \frac{d\lambda_{rq}}{dt} - \omega\lambda_{rd} \tag{2.18}$$

$$\frac{d\theta}{dt} = \omega \tag{2.19}$$

$$\frac{J}{p/2}\frac{d\omega}{dt} = T_e - T_m \tag{2.20}$$

where $v_{sd} = v_{sa}$, $i_{sd} = i_{sa}$, and $\lambda_{sd} = \lambda_{sa}$. The new flux-current relationships are given by

$$\begin{bmatrix} \lambda_{sd} \\ \lambda_{rd} \\ \lambda_{rq} \end{bmatrix} = \begin{bmatrix} L_{\ell s} + L_{ms} & L_{ms} & 0 \\ L_{ms} & L_{\ell r} + L_{ms} & 0 \\ 0 & 0 & L_{\ell r} + L_{ms} \end{bmatrix} \begin{bmatrix} i_{sd} \\ i_{rd} \\ i_{rq} \end{bmatrix} \tag{2.21}$$

and the electromagnetic torque simplifies to

$$T_e = -\left(\frac{p}{2}\right) L_{ms} i_{sd} i_{rq}. \tag{2.22}$$

This model is expressed using flux linkages and inductances. By using the following transformation matrix, the model is now expressed in terms of voltage variables and reactances as

$$\begin{bmatrix} \psi_{sd} \\ \psi_{rd} \\ \psi_{rq} \end{bmatrix} = \omega_s \begin{bmatrix} \lambda_{sd} \\ \lambda_{rd} \\ \lambda_{rq} \end{bmatrix} = \begin{bmatrix} X_{\ell s} + X_{ms} & X_{ms} & 0 \\ X_{ms} & X_{\ell r} + X_{ms} & 0 \\ 0 & 0 & X_{\ell r} + X_{ms} \end{bmatrix} \begin{bmatrix} i_{sd} \\ i_{rd} \\ i_{rq} \end{bmatrix} \tag{2.23}$$

where $\omega_s = 120\pi$ and 60-Hz reactances have been substituted for inductances. The final model in dq-coordinates is given by

$$v_{sd} = R_s i_{sd} + \frac{1}{\omega_s} \frac{d\psi_{sd}}{dt} \tag{2.24}$$

$$0 = R_r i_{rd} + \frac{1}{\omega_s} \frac{d\psi_{rd}}{dt} + \frac{\omega}{\omega_s} \psi_{rq} \tag{2.25}$$

$$0 = R_r i_{rq} + \frac{1}{\omega_s} \frac{d\psi_{rq}}{dt} - \frac{\omega}{\omega_s} \psi_{rd} \tag{2.26}$$

$$\frac{d\theta}{dt} = \omega \tag{2.27}$$

$$\frac{J}{p/2} \frac{d\omega}{dt} = T_e - T_m \tag{2.28}$$

along with the new flux-current relationships

$$\begin{bmatrix} \psi_{sd} \\ \psi_{rd} \\ \psi_{rq} \end{bmatrix} = \begin{bmatrix} X_{\ell s} + X_{ms} & X_{ms} & 0 \\ X_{ms} & X_{\ell r} + X_{ms} & 0 \\ 0 & 0 & X_{\ell r} + X_{ms} \end{bmatrix} \begin{bmatrix} i_{sd} \\ i_{rd} \\ i_{rq} \end{bmatrix}. \tag{2.29}$$

The electromagnetic torque expression using reactances becomes

$$T_e = -\left(\frac{p}{2}\right)\left(\frac{X_{ms}}{\omega_s}\right) i_{sd} i_{rq}. \tag{2.30}$$

Next, an alternative model found in reference [8] is obtained where the q-axis aligned with the sa-axis. Consider the q-axis in Figure 2.3, where now it is aligned with sa-axis.

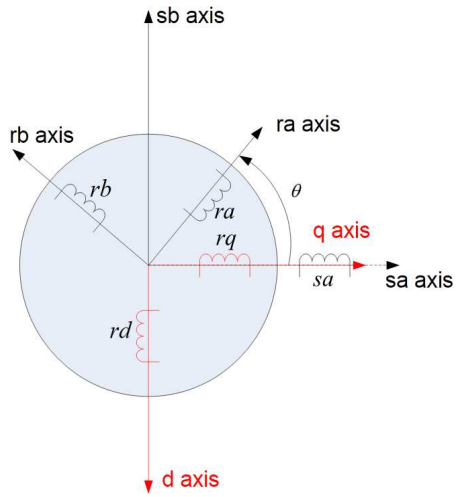

Figure 2.3: Stator and Rotor Windings in dq Coordinate

The new dq transformations are

$$\begin{bmatrix} i_{rq} \\ i_{rd} \end{bmatrix} = \begin{bmatrix} \cos\theta & -\sin\theta \\ -\sin\theta & -\cos\theta \end{bmatrix} \begin{bmatrix} i_{ra} \\ i_{rb} \end{bmatrix} \tag{2.31}$$

and for currents and

$$\begin{bmatrix} \psi_{rq} \\ \psi_{rd} \end{bmatrix} = \begin{bmatrix} \cos\theta & -\sin\theta \\ -\sin\theta & -\cos\theta \end{bmatrix} \begin{bmatrix} \psi_{ra} \\ \psi_{rb} \end{bmatrix}. \tag{2.32}$$

for fluxes. Equations (2.31) and (2.32) are the new transformations with the q-axis aligned with the sa-axis. The final model in these dq coordinates is given by

$$v_{sq} = R_s i_{sq} + \frac{1}{\omega_s}\frac{d\psi_{sq}}{dt} \tag{2.33}$$

$$0 = R_r i_{rd} + \frac{1}{\omega_s}\frac{d\psi_{rd}}{dt} + \frac{\omega}{\omega_s}\psi_{rq} \tag{2.34}$$

$$0 = R_r i_{rq} + \frac{1}{\omega_s}\frac{d\psi_{rq}}{dt} - \frac{\omega}{\omega_s}\psi_{rd} \tag{2.35}$$

$$\frac{d\theta}{dt} = \omega \tag{2.36}$$

$$\frac{J}{p/2}\frac{d\omega}{dt} = T_e - T_m \tag{2.37}$$

where $v_{sq} = v_{sa}$, $i_{sq} = i_{sa}$, $\psi_{sq} = \psi_{sa}$, and

$$T_e = \left(\frac{p}{2}\right)\left(\frac{X_{ms}}{\omega_s}\right) i_{sq} i_{rd} \tag{2.38}$$

along with the flux-current relationships

$$\begin{bmatrix} \psi_{sq} \\ \psi_{rq} \\ \psi_{rd} \end{bmatrix} = \begin{bmatrix} X_{\ell s} + X_{ms} & X_{ms} & 0 \\ X_{ms} & X_{\ell r} + X_{ms} & 0 \\ 0 & 0 & X_{\ell r} + X_{ms} \end{bmatrix} \begin{bmatrix} i_{sq} \\ i_{rq} \\ i_{rd} \end{bmatrix}. \tag{2.39}$$

2.3 Augmented Dynamic Model of a Single-Phase Induction Machine

To develop an augmented model, a stationary dq reference frame is used in this thesis, where the d-axis is aligned with sa-axis. To lighten up the notation, new current variables are defined as

$$i_s = i_{sd} \tag{2.40}$$

$$i_d = i_{rd} \tag{2.41}$$

$$i_q = i_{rq} \tag{2.42}$$

and similarly for flux linkages and voltage variables. The stator winding is excited with a sinusoidal source voltage of the form

$$v_s(t) = \sqrt{2}V_s \cos\omega_s t = \sqrt{2}\left(\frac{V_s}{2}\right)e^{j\omega_s t} + \sqrt{2}\left(\frac{V_s}{2}\right)e^{-j\omega_s t}. \tag{2.43}$$

The existence of current solutions is postulated for $i_s(t)$, $i_d(t)$, and $i_q(t)$ in the form

$$i_s(t) = \sqrt{2}\left(\frac{I_s(t)}{2}\right)e^{j\omega_s t} + \sqrt{2}\left(\frac{I_s^*(t)}{2}\right)e^{-j\omega_s t} \tag{2.44}$$

$$i_d(t) = \sqrt{2}\left(\frac{I_d(t)}{2}\right)e^{j\omega_s t} + \sqrt{2}\left(\frac{I_d^*(t)}{2}\right)e^{-j\omega_s t} \tag{2.45}$$

$$i_q(t) = \sqrt{2}\left(\frac{I_q(t)}{2}\right)e^{j\omega_s t} + \sqrt{2}\left(\frac{I_q^*(t)}{2}\right)e^{-j\omega_s t}. \tag{2.46}$$

where the new complex current solutions are defined in capital letters by I_s, I_d, and I_q. It can be similarly verified that the fluxes ψ_s, ψ_d, and ψ_q can also be expressed as

$$\psi_s(t) = \sqrt{2}\left(\frac{\Psi_s(t)}{2}\right)e^{j\omega_s t} + \sqrt{2}\left(\frac{\Psi_s^*(t)}{2}\right)e^{-j\omega_s t} \quad (2.47)$$

$$\psi_d(t) = \sqrt{2}\left(\frac{\Psi_d(t)}{2}\right)e^{j\omega_s t} + \sqrt{2}\left(\frac{\Psi_d^*(t)}{2}\right)e^{-j\omega_s t} \quad (2.48)$$

$$\psi_q(t) = \sqrt{2}\left(\frac{\Psi_q(t)}{2}\right)e^{j\omega_s t} + \sqrt{2}\left(\frac{\Psi_q^*(t)}{2}\right)e^{-j\omega_s t} \quad (2.49)$$

where

$$\begin{bmatrix}\Psi_s\\ \Psi_d\\ \Psi_q\end{bmatrix} = \begin{bmatrix}X_{\ell s}+X_{ms} & X_{ms} & 0\\ X_{ms} & X_{\ell r}+X_{ms} & 0\\ 0 & 0 & X_{\ell r}+X_{ms}\end{bmatrix}\begin{bmatrix}I_s\\ I_d\\ I_q\end{bmatrix}. \quad (2.50)$$

Substituting Equations (2.47) through (2.49) into (2.33) yields

$$\begin{aligned}\sqrt{2}\left(\frac{V_s}{2}\right)e^{j\omega_s t} + \sqrt{2}\left(\frac{V_s}{2}\right)e^{-j\omega_s t} &= R_s\left[\sqrt{2}\left(\frac{I_s(t)}{2}e^{j\omega_s t}\right) + \sqrt{2}\left(\frac{I_s^*(t)}{2}e^{-j\omega_s t}\right)\right]\\ &+ \frac{1}{\omega_s}\frac{d}{dt}\left[\sqrt{2}\left(\frac{\Psi_s(t)}{2}e^{j\omega_s t}\right) + \sqrt{2}\left(\frac{\Psi_s^*(t)}{2}e^{-j\omega_s t}\right)\right]. \quad (2.51)\end{aligned}$$

After identifying the coefficients of the linearly-independent functions $e^{j\omega_s t}$ and $e^{-j\omega_s t}$, the above differential equation simplify to

$$V_s = R_s I_s + \frac{1}{\omega_s}\frac{d\Psi_s}{dt} + j\Psi_s. \quad (2.52)$$

Repeating this process for the rotor and the speed equations, we end up with the following fourth-order complex differential model of a single-phase induction machine

$$
\begin{aligned}
V_s &= R_s I_s + \frac{1}{\omega_s}\frac{d\Psi_s}{dt} + j\Psi_s && (2.53)\\
0 &= R_r I_d + \frac{1}{\omega_s}\frac{d\Psi_d}{dt} + j\Psi_d + \frac{\omega}{\omega_s}\Psi_q && (2.54)\\
0 &= R_r I_q + \frac{1}{\omega_s}\frac{d\Psi_q}{dt} + j\Psi_q - \frac{\omega}{\omega_s}\Psi_d && (2.55)\\
\frac{J}{(p/2)}\frac{d\omega}{dt} &= -\left(\frac{1}{2}\right)\left(\frac{p}{2}\right)\left(\frac{X_m}{\omega_s}\right)[I_s I_q^* + I_s^* I_q \\
&\quad + I_s I_q e^{j2\omega_s t} + I_s^* I_q^* e^{-j2\omega_s t}] - T_m. && (2.56)
\end{aligned}
$$

2.4 Averaged Dynamic Model of a Single-Phase Induction Machine

After averaging the right-hand sides of (2.53)-(2.56) with respect to time t as explained in Appendix A, the following autonomous system is obtained

$$
\begin{aligned}
\frac{1}{\omega_s}\frac{d\bar{\Psi}_s}{dt} &= -R_s\bar{I}_s - j\bar{\Psi}_s + V_s && (2.57)\\
\frac{1}{\omega_s}\frac{d\bar{\Psi}_d}{dt} &= -R_r\bar{I}_d - j\bar{\Psi}_d - \frac{\omega}{\omega_s}\bar{\Psi}_q && (2.58)\\
\frac{1}{\omega_s}\frac{d\bar{\Psi}_q}{dt} &= -R_r\bar{I}_q - j\bar{\Psi}_q + \frac{\omega}{\omega_s}\bar{\Psi}_d && (2.59)\\
\frac{J}{(p/2)}\frac{d\omega}{dt} &= -\left(\frac{1}{2}\right)\left(\frac{p}{2}\right)\left(\frac{X_{ms}}{\omega_s}\right)\left[\bar{I}_s\bar{I}_q^* + \bar{I}_s^*\bar{I}_q\right] - T_m && (2.60)
\end{aligned}
$$

where $\bar{\Psi}$ and $\bar{I}$ denote the time averaged quantities of the corresponding flux and current variables, respectively. The constitutive flux-current relationships remain the same, i.e.,

$$
\begin{bmatrix}\bar{\Psi}_s\\ \bar{\Psi}_d\\ \bar{\Psi}_q\end{bmatrix} = \begin{bmatrix}X_{\ell s}+X_{ms} & X_{ms} & 0\\ X_{ms} & X_{\ell r}+X_{ms} & 0\\ 0 & 0 & X_{\ell r}+X_{ms}\end{bmatrix}\begin{bmatrix}\bar{I}_s\\ \bar{I}_d\\ \bar{I}_q\end{bmatrix}. \qquad (2.61)
$$

In order to simulate Equations (2.57) through (2.60), they need to be written in terms of seven real state variables as $(\psi_{sx}, \psi_{sy}, \psi_{dx}, \psi_{dy}, \psi_{qx}, \psi_{qy}, \omega)$. This model will be referred to as the averaged seventh-order dq-model:

$$\frac{1}{\omega_s}\frac{d\Psi_{sx}}{dt} = -R_s I_{sx} + \Psi_{sy} + V_{sx} \tag{2.62}$$

$$\frac{1}{\omega_s}\frac{d\Psi_{sy}}{dt} = -R_s I_{sy} - \Psi_{sx} + V_{sy} \tag{2.63}$$

$$\frac{1}{\omega_s}\frac{d\Psi_{dx}}{dt} = -R_r I_{dx} + \Psi_{dy} - \frac{\omega}{\omega_s}\Psi_{qx} \tag{2.64}$$

$$\frac{1}{\omega_s}\frac{d\Psi_{dy}}{dt} = -R_r I_{dy} - \Psi_{dx} - \frac{\omega}{\omega_s}\Psi_{qy} \tag{2.65}$$

$$\frac{1}{\omega_s}\frac{d\Psi_{qx}}{dt} = -R_r I_{qx} + \Psi_{qx} + \frac{\omega}{\omega_s}\Psi_{dx} \tag{2.66}$$

$$\frac{1}{\omega_s}\frac{d\Psi_{qy}}{dt} = -R_r I_{qy} - \Psi_{qy} + \frac{\omega}{\omega_s}\Psi_{dy} \tag{2.67}$$

$$\frac{J}{(p/2)}\frac{d\omega}{dt} = -\left(\frac{p}{2}\right)\left(\frac{X_m}{\omega_s}\right)(I_{sx}I_{qx} + I_{sy}I_{qy}) - T_m \tag{2.68}$$

with the following flux-current relationships

$$\begin{bmatrix} \Psi_{sx} \\ \Psi_{sy} \\ \Psi_{dx} \\ \Psi_{dy} \\ \Psi_{qx} \\ \Psi_{qy} \end{bmatrix} = \begin{bmatrix} X_s & 0 & X_{ms} & 0 & 0 & 0 \\ 0 & X_s & 0 & X_{ms} & 0 & 0 \\ X_{ms} & 0 & X_r & 0 & 0 & 0 \\ 0 & X_{ms} & 0 & X_r & 0 & 0 \\ 0 & 0 & 0 & 0 & X_r & 0 \\ 0 & 0 & 0 & 0 & 0 & X_r \end{bmatrix} \begin{bmatrix} I_{sx} \\ I_{sy} \\ I_{dx} \\ I_{dy} \\ I_{qx} \\ I_{qy} \end{bmatrix} \tag{2.69}$$

where $X_s = X_{\ell s} + X_{ms}$ and $X_r = X_{\ell r} + X_{ms}$.

2.5 Model with Forward- and Backward-Rotating Components

The obtained dq-model is now transformed to new coordinates with forward- and backward-rotating components. Forward and backward flux variables are defined as

$$\begin{bmatrix} \bar{\Psi}_f \\ \bar{\Psi}_b \end{bmatrix} = \frac{1}{2} \begin{bmatrix} 1 & j \\ 1 & -j \end{bmatrix} \begin{bmatrix} \bar{\Psi}_d \\ \bar{\Psi}_q \end{bmatrix} \tag{2.70}$$

Similarly, forward and backward current variables are defined as

$$\begin{bmatrix} \bar{I}_f \\ \bar{I}_b \end{bmatrix} = \begin{bmatrix} 1 & j \\ 1 & -j \end{bmatrix} \begin{bmatrix} \bar{I}_d \\ \bar{I}_q \end{bmatrix}. \tag{2.71}$$

The above transformation matrices have been defined differently for fluxes (or voltages) and currents in order to preserve power invariance in the two models. The inverse transformations are

$$\begin{bmatrix} \bar{\Psi}_d \\ \bar{\Psi}_q \end{bmatrix} = \begin{bmatrix} 1 & 1 \\ -j & j \end{bmatrix} \begin{bmatrix} \bar{\Psi}_f \\ \bar{\Psi}_b \end{bmatrix} \tag{2.72}$$

and

$$\begin{bmatrix} \bar{I}_d \\ \bar{I}_q \end{bmatrix} = \frac{1}{2} \begin{bmatrix} 1 & 1 \\ -j & j \end{bmatrix} \begin{bmatrix} \bar{I}_f \\ \bar{I}_b \end{bmatrix}. \tag{2.73}$$

Using Equations (2.70) through (2.73), a new complex model with forward and backward components is obtained as

$$\frac{1}{\omega_s}\frac{d\bar{\Psi}_s}{dt} = V_s - R_s\bar{I}_s - j\bar{\Psi}_s \tag{2.74}$$

$$\frac{1}{\omega_s}\frac{d\bar{\Psi}_f}{dt} = -\frac{R_r}{2}\bar{I}_f - j\left(\frac{\omega_s-\omega}{\omega_s}\right)\bar{\Psi}_f \tag{2.75}$$

$$\frac{1}{\omega_s}\frac{d\bar{\Psi}_b}{dt} = -\frac{R_r}{2}\bar{I}_b - j\left(\frac{\omega_s+\omega}{\omega_s}\right)\bar{\Psi}_b \tag{2.76}$$

$$\frac{J}{(p/2)}\frac{d\omega}{dt} = -\left(\frac{p}{2}\right)\left(\frac{X_{ms}}{\omega_s}\right)\left(\frac{1}{2}\right)\left[\frac{\bar{I}_s}{2}\left(-j\bar{I}_f + j\bar{I}_b\right)^* + \frac{\bar{I}_s^*}{2}\left(-j\bar{I}_f + j\bar{I}_b\right)\right] - T_m \tag{2.77}$$

In order to simulate this model, real and imaginary flux and current components are defined as

$$\bar{\Psi}_s = \Psi_{sx} + j\Psi_{sy} \tag{2.78}$$

$$\bar{\Psi}_f = \Psi_{fx} + j\Psi_{fy} \tag{2.79}$$

$$\bar{\Psi}_b = \Psi_{bx} + j\Psi_{by} \tag{2.80}$$

and

$$\bar{I}_s = I_{sx} + jI_{sy} \tag{2.81}$$

$$\bar{I}_f = I_{fx} + jI_{fy} \tag{2.82}$$

$$\bar{I}_b = I_{bx} + jI_{by}. \tag{2.83}$$

Use of the above transformations yields the final model below,

$$\frac{1}{\omega_s}\frac{d\Psi_{sx}}{dt} = -R_s I_{sx} + V_{sx} + \Psi_{sy} \tag{2.84}$$

$$\frac{1}{\omega_s}\frac{d\Psi_{sy}}{dt} = -R_s I_{sy} + V_{sy} - \Psi_{sx} \tag{2.85}$$

$$\frac{1}{\omega_s}\frac{d\Psi_{fx}}{dt} = -\frac{R_r}{2} I_{fx} + \left(\frac{\omega_s - \omega}{\omega_s}\right)\Psi_{fy} \tag{2.86}$$

$$\frac{1}{\omega_s}\frac{d\Psi_{fy}}{dt} = -\frac{R_r}{2} I_{fy} - \left(\frac{\omega_s - \omega}{\omega_s}\right)\Psi_{fx} \tag{2.87}$$

$$\frac{1}{\omega_s}\frac{d\Psi_{bx}}{dt} = -\frac{R_r}{2} I_{bx} + \left(\frac{\omega_s + \omega}{\omega_s}\right)\Psi_{by} \tag{2.88}$$

$$\frac{1}{\omega_s}\frac{d\Psi_{by}}{dt} = -\frac{R_r}{2} I_{by} - \left(\frac{\omega_s + \omega}{\omega_s}\right)\Psi_{bx} \tag{2.89}$$

$$\frac{J}{(p/2)}\frac{d\omega}{dt} = -\left(\frac{p}{2}\right)\left(\frac{X_{ms}}{\omega_s}\right)\left(\frac{1}{2}\right)\left[I_{sx}I_{fy} - I_{sy}I_{fx} + I_{sy}I_{bx} - I_{sx}I_{by}\right] - T_m \tag{2.90}$$

along with its flux-current relationships,

$$\begin{bmatrix} \Psi_{sx} \\ \Psi_{sy} \\ \Psi_{fx} \\ \Psi_{fy} \\ \Psi_{bx} \\ \Psi_{by} \end{bmatrix} = \begin{bmatrix} X_s & 0 & \frac{X_{ms}}{2} & 0 & \frac{X_{ms}}{2} & 0 \\ 0 & X_s & 0 & \frac{X_r}{2} & 0 & \frac{X_r}{2} \\ \frac{X_{ms}}{2} & 0 & \frac{X_r}{2} & 0 & 0 & 0 \\ 0 & \frac{X_{ms}}{2} & 0 & \frac{X_r}{2} & 0 & 0 \\ \frac{X_{ms}}{2} & 0 & 0 & 0 & \frac{X_r}{2} & 0 \\ 0 & \frac{X_{ms}}{2} & 0 & 0 & 0 & \frac{X_r}{2} \end{bmatrix} \begin{bmatrix} I_{sx} \\ I_{sy} \\ I_{fx} \\ I_{fy} \\ I_{bx} \\ I_{by} \end{bmatrix} \tag{2.91}$$

This model will be referred to as the averaged seventh-order fb-model.

2.6 Steady-State Equivalent Circuit

The traditional quasi-steady-state circuit can be derived using several methods in the literature [6]. The equations of the previous section are now used to derive this circuit.

This circuit is based on the forward and backward components. The quasi-steady-state algebraic equations corresponding to Equations (2.74) through (2.76) are obtained as

$$0 = V_s - R_s\bar{I}_s - j\bar{\Psi}_s \tag{2.92}$$

$$0 = -\frac{R_r}{2}\bar{I}_f - j\left(\frac{\omega_s - \omega}{\omega_s}\right)\bar{\Psi}_f \tag{2.93}$$

$$0 = -\frac{R_r}{2}\bar{I}_b - j\left(\frac{\omega_s + \omega}{\omega_s}\right)\bar{\Psi}_b. \tag{2.94}$$

Recalling the flux-current relations as

$$\bar{\Psi}_s = (X_{\ell s} + X_{ms})\bar{I}_s + j\frac{X_{ms}}{2}\bar{I}_f + j\frac{X_{ms}}{2}\bar{I}_b \tag{2.95}$$

$$\bar{\Psi}_f = j\frac{X_{ms}}{2}\bar{I}_s + j\left(\frac{X_{\ell r}}{2} + \frac{X_{ms}}{2}\right)\bar{I}_f \tag{2.96}$$

$$\bar{\Psi}_b = j\frac{X_{ms}}{2}\bar{I}_s + j\left(\frac{X_{\ell r}}{2} + \frac{X_{ms}}{2}\right)\bar{I}_b \tag{2.97}$$

and substituting these relations into Equations (2.92)-(2.94) yields the standard quasi-steady-state of a single-phase induction machine shown in Figure 2.4 and where

$$s = \frac{\omega_s - \omega}{\omega_s}. \tag{2.98}$$

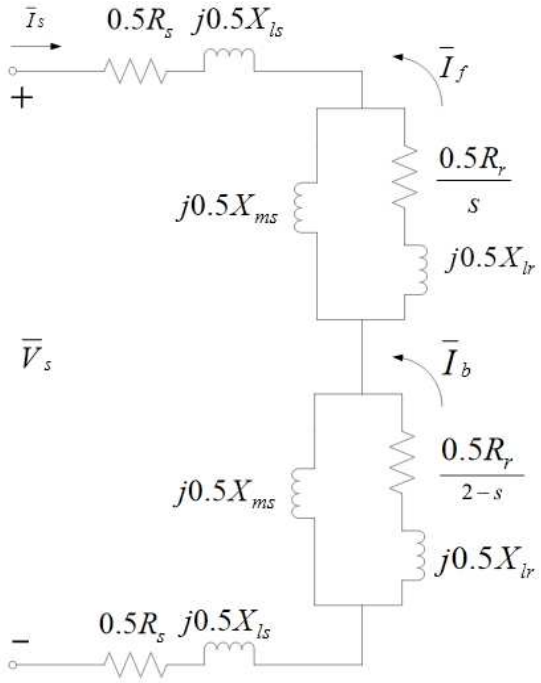

Figure 2.4: Equivalent Circuit Representation of a Single-Phase Induction Motor

The electromagnetic torque T_e is calculated using forward- and backward-rotating components computed from the equivalent circuit of Figure 2.4 using the following formulas [6]':

$$T_{ef} = \frac{p}{2}\frac{R_r I_f^2}{2s\omega_s} \tag{2.99}$$

$$T_{eb} = \frac{p}{2}\frac{R_r I_b^2}{2(2-s)\omega_s} \tag{2.100}$$

$$T_e = T_{ef} - T_{eb}. \tag{2.101}$$

CHAPTER 3

MODELING OF TWO THREE-PHASE SERIES-CONNECTED INDUCTION MACHINES

In the previous chapter, the averaged seventh-order model of an induction machine was derived and expressed in terms of forward and backward components. In this chapter, it is proved that this model is dynamically equivalent to the model of two three-phase induction machines connected in series but with opposite stator phase sequences. The characteristics of this new model will be investigated and compared to the averaged seventh-order of a single-phase induction machine. For the sake of consistency, both models will be studied in the synchronously-rotating reference frame.

3.1 Series-Connected Induction Machines

Figure 3.1 shows two identical three-phase induction machines with their stator windings connected in series but with opposite stator phase sequences. Each box represents a machine with its own stator and rotor windings.

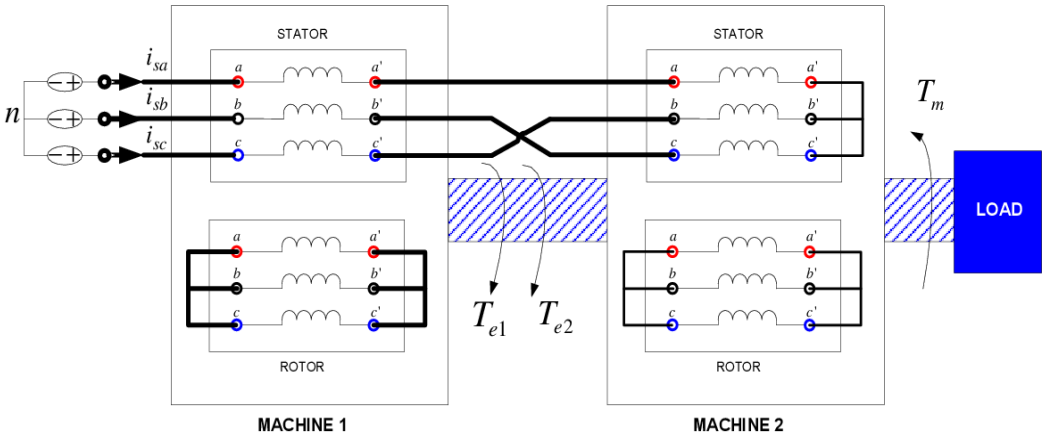

Figure 3.1: Two Three-Phase Induction Machines Connected in Series

The rotor windings of each machine are shorted out. From Figure 3.1, it is easily seen that

$$i_{sa} = i_{sa1} = i_{sa2} \tag{3.1}$$

$$i_{sb} = i_{sb1} = i_{sc2} \tag{3.2}$$

$$i_{sc} = i_{sc1} = i_{sb2} \tag{3.3}$$

where i_{sa}, i_{sb}, and i_{sc} are the source currents. Similarly, i_{sa1}, i_{sb1}, and i_{sc1} are the *abc* stator currents of machine 1, and i_{sa2}, i_{sb2}, and i_{sc2} are the *abc* stator currents of machine 2. In space vector form,

$$\vec{i}_s = \frac{2}{3}(i_{sa} + \bar{a}i_{sb} + \bar{a}^2 i_{sc}) = \vec{i}_{s1} = \vec{i}^*_{s2} \tag{3.4}$$

where $\bar{a} = 1\angle 120^o$ and $\vec{i}^*_{s2}$ is the complex conjugate of $\vec{i}_{s2}$. The dynamic equations of machine 1 are expressed in terms of its stator and rotor fluxes and currents as

$$\vec{v}_{s1} = R_s\vec{i}_{s1} + \frac{d\vec{\lambda}_{s1}}{dt} \tag{3.5}$$

$$0 = R_r\vec{i}_{r1} + \frac{d\vec{\lambda}_{r1}}{dt}. \tag{3.6}$$

From Appendix B,

$$\vec{\lambda}_{s1} = (L_{\ell s} + \frac{3}{2}L_{ms})\vec{i}_{s1} + \frac{3}{2}L_{ms}e^{j\theta_1}\vec{i}_{r1} \tag{3.7}$$

$$\vec{\lambda}_{r1} = \frac{3}{2}L_{ms}\vec{i}_{s1}e^{-j\theta_1} + (L_{\ell r} + \frac{3}{2}L_{ms})\vec{i}_{r1} \tag{3.8}$$

Defining $\vec{\lambda}'_{r1} = \vec{\lambda}_{r1}e^{j\theta_1}$, we obtain the derivative of $\vec{\lambda}'_{r1}$ as

$$\frac{d\vec{\lambda}'_{r1}}{dt} = \frac{d}{dt}(\vec{\lambda}_{r1}e^{j\theta_1}) = \frac{d\vec{\lambda}_{r1}}{dt}e^{j\theta_1} + j\omega_1\vec{\lambda}_{r1}e^{j\theta_1} \tag{3.9}$$

Using Equations (3.6) and (3.9),

$$\frac{d\vec{\lambda}'_{r1}}{dt} = -R_r\vec{i}'_{r1} + j\omega_1\vec{\lambda}'_{r1} \tag{3.10}$$

where $\vec{i}'_{r1} = \vec{i}_{r1}e^{j\theta_1}$. To sum up these results, the voltage equations for machine 1 are given by

$$\vec{v}_{s1} = R_s\vec{i}_{s1} + \frac{d\vec{\lambda}'_{s1}}{dt} \tag{3.11}$$

$$\frac{d\vec{\lambda}'_{r1}}{dt} = -R_r\vec{i}'_{r1} + j\omega_1\vec{\lambda}'_{r1} \tag{3.12}$$

along with the flux-current relationships

$$\vec{\lambda}_{s1} = (L_{\ell s} + \frac{3}{2}L_{ms})\vec{i}_{s1} + \frac{3}{2}L_{ms}\vec{i}'_{r1} \quad (3.13)$$

$$\vec{\lambda}'_{r1} = \frac{3}{2}L_{ms}\vec{i}_{s1} + (L_{\ell r} + \frac{3}{2}L_{ms})\vec{i}'_{r1}. \quad (3.14)$$

Similarly, the voltage equations of machine 2 are given by

$$\vec{v}_{s2} = R_s\vec{i}_{s2} + \frac{d\vec{\lambda}_{s2}}{dt} \quad (3.15)$$

$$\frac{d\vec{\lambda}'_{r2}}{dt} = -R'_r\vec{i}'_{r2} + j\omega_2\vec{\lambda}'_{r2} \quad (3.16)$$

along with the new flux-current relationships

$$\vec{\lambda}_{s2} = (L_{\ell s} + \frac{3}{2}L_{ms})\vec{i}_{s2} + \frac{3}{2}L_{ms}\vec{i}'_{r2} \quad (3.17)$$

$$\vec{\lambda}'_{r2} = \frac{3}{2}L_{ms}\vec{i}_{s2} + (L_{\ell s} + \frac{3}{2}L_{ms})\vec{i}'_{r2} \quad (3.18)$$

where $\vec{\lambda}'_{r2} = \vec{\lambda}_{r2}e^{j\theta_2}$ and $\vec{i}'_{r2} = \vec{i}_{r2}e^{j\theta_2}$. With both machines connected in series through their stator windings, the applied stator voltage $\vec{v}_s$ can be expressed as

$$\vec{v}_s = \vec{v}_{s1} + \vec{v}^*_{s2} = R_s\vec{i}_{s1} + \frac{d\vec{\lambda}_{s1}}{dt} + R_s\vec{i}^*_{s2} + \frac{d\vec{\lambda}^*_{s2}}{dt}. \quad (3.19)$$

Since $\vec{i}_s = \vec{i}_{s1} = \vec{i}^*_{s2}$, we have

$$\vec{v}_s = 2R_s\vec{i}_s + \frac{d\vec{\lambda}_s}{dt} \quad (3.20)$$

where the total flux linkages is defined as $\vec{\lambda}_s = \vec{\lambda}_{s1} + \vec{\lambda}^*_{s2}$. Using Equations (3.13) and (3.17), this total flux can be expressed in terms of currents as

$$\vec{\lambda}_s = \vec{\lambda}_{s1} + \vec{\lambda}^*_{s2} = 2(L_{\ell s} + \frac{3}{2}L_{ms})\vec{i}_s + \frac{3}{2}L_{ms}\vec{i}'_{r1} + \frac{3}{2}L_{ms}\vec{i}'^*_{r2}. \quad (3.21)$$

The rotor voltage equations remain as they are, that is,

$$0 = R_r\vec{i}'_{r1} + \frac{d\vec{\lambda}'_{r1}}{dt} - j\omega_1\vec{\lambda}'_{r1} \tag{3.22}$$

$$0 = R_r\vec{i}'^{*}_{r2} + \frac{d\vec{\lambda}'^{*}_{r2}}{dt} - j\omega_2\vec{\lambda}'^{*}_{r2} \tag{3.23}$$

To sum up, the series-connected induction machines are modeled by the following complex differential voltage equations

$$\vec{v}_s = 2R_s\vec{i}_s + \frac{d\vec{\lambda}_s}{dt} \tag{3.24}$$

$$0 = R_r\vec{i}'_{r1} + \frac{d\vec{\lambda}'_{r1}}{dt} - j\omega_1\vec{\lambda}'_{r1} \tag{3.25}$$

$$0 = R_r\vec{i}'^{*}_{r2} + \frac{d\vec{\lambda}'^{*}_{r2}}{dt} - j\omega_2\vec{\lambda}'^{*}_{r2} \tag{3.26}$$

together with the flux-current relationships

$$\vec{\lambda}_s = 2(L_{\ell s} + \frac{3}{2}L_{ms})\vec{i}_s + \frac{3}{2}L_{ms}\vec{i}'_{r1} + \frac{3}{2}L_{ms}\vec{i}'^{*}_{r2} \tag{3.27}$$

$$\vec{\lambda}'_{r1} = \frac{3}{2}L_{ms}\vec{i}_s + (L_{\ell r} + \frac{3}{2}L_{ms})\vec{i}'_{r1} \tag{3.28}$$

$$\vec{\lambda}'_{r2} = \frac{3}{2}L_{ms}\vec{i}_s + (L_{\ell s} + \frac{3}{2}L_{ms})\vec{i}'_{r2}. \tag{3.29}$$

3.1.1 Mathematical Model of Two Series-Connected Three-Phase Induction Machines in dq-Coordinates

The previous model is now transformed into dq-coordinates by decomposing all fluxes and currents into real (d) and imaginary (q) components. Defining

$$\vec{\lambda}_s = \lambda_{sd} + j\lambda_{sq} \tag{3.30}$$

$$\vec{\lambda}_{r1} = \lambda_{rd1} + j\lambda_{rq1} \tag{3.31}$$

$$\vec{\lambda}_{r2} = \lambda_{rd2} + j\lambda_{rq2} \tag{3.32}$$

for fluxes and

$$\vec{i}_s = i_{sd} + ji_{sq} \tag{3.33}$$

$$\vec{i}_{r1} = i_{rd1} + ji_{rq1} \tag{3.34}$$

$$\vec{i}_{r2} = i_{rd2} + ji_{rq2}. \tag{3.35}$$

for currents, and substituting Equations (3.30) to (3.35) into Equation (3.27), yields

$$\begin{aligned} \vec{\lambda}_s = \lambda_{sd} + j\lambda_{sq} &= 2(L_{\ell s} + \frac{3}{2}L_{ms})(i_{sd} + ji_{sq}) + \frac{3}{2}L_{ms}(i_{rd1} + ji_{rq1}) \\ &\quad + \frac{3}{2}L_{ms}(i_{rd2} - ji_{rq2}). \end{aligned} \tag{3.36}$$

Collecting real and imaginary components on both sides of this equation, we obtain

$$\lambda_{sd} = 2(L_{\ell s} + \frac{3}{2}L_{ms})i_{sd} + \frac{3}{2}L_{ms}i_{rd1} + \frac{3}{2}L_{ms}i_{rd2} \tag{3.37}$$

$$\lambda_{sq} = 2(L_{\ell s} + \frac{3}{2}L_{ms})i_{sq} + \frac{3}{2}L_{ms}i_{rq1} - \frac{3}{2}L_{ms}i_{rq2}. \tag{3.38}$$

A similar decomposition of the rotor flux $\vec{\lambda}'_{r1}$ of machine 1 yields

$$\vec{\lambda}'_{r1} = \lambda_{rd1} + j\lambda_{rq1} = \frac{3}{2}L_{ms}(i_{sd} + ji_{sq}) + (L_{\ell r} + \frac{3}{2}L_{ms})(i_{rd1} + ji_{rq1}) \tag{3.39}$$

and

$$\lambda_{rd1} = \frac{3}{2}L_{ms}i_{sd} + (L_{\ell r} + \frac{3}{2}L_{ms})i_{rd1} \tag{3.40}$$

$$\lambda_{rq1} = \frac{3}{2}L_{ms}i_{sq} + (L_{\ell r} + \frac{3}{2}L_{ms})i_{rq1}. \tag{3.41}$$

Applying the same procedure for the rotor flux $\vec{\lambda}'_{r2}$ of machine 2 yields

$$\vec{\lambda}'_{r2} = (\lambda_{rd2} + j\lambda_{rq2}) = \frac{3}{2}L_{ms}(i_{sd} - ji_{sq}) + (L_{\ell r} + \frac{3}{2}L_{ms})(i_{rd2} + ji_{rq2}) \tag{3.42}$$

and

$$\lambda_{rd2} = \frac{3}{2}L_{ms}i_{sd} + (L_{\ell r} + \frac{3}{2}L_{ms})i_{rd2} \tag{3.43}$$

$$\lambda_{rq2} = -\frac{3}{2}L_{ms}i_{sq} + (L_{\ell r} + \frac{3}{2}L_{ms})i_{rq2}. \tag{3.44}$$

After decomposing all space vector fluxes into real and imaginary components, the flux-current relationships for the d-axis are given by

$$\begin{bmatrix} \lambda_{sd} \\ \lambda_{rd1} \\ \lambda_{rd2} \end{bmatrix} = \begin{bmatrix} 2(L_{\ell s} + \frac{3}{2}L_{ms}) & \frac{3}{2}L_{ms} & \frac{3}{2}L_{ms} \\ \frac{3}{2}L_{ms} & (L_{\ell r} + \frac{3}{2}L_{ms}) & 0 \\ \frac{3}{2}L_{ms} & 0 & (L_{\ell r} + \frac{3}{2}L_{ms}) \end{bmatrix} \begin{bmatrix} i_{sd} \\ i_{rd1} \\ i_{rd2} \end{bmatrix} \tag{3.45}$$

and

$$\begin{bmatrix} \lambda_{sq} \\ \lambda_{rq1} \\ \lambda_{rq2} \end{bmatrix} = \begin{bmatrix} 2(L_{\ell s} + \frac{3}{2}L_{ms}) & \frac{3}{2}L_{ms} & -\frac{3}{2}L_{ms} \\ \frac{3}{2}L_{ms} & (L_{\ell r} + \frac{3}{2}L_{ms}) & 0 \\ -\frac{3}{2}L_{ms} & 0 & (L_{\ell r} + \frac{3}{2}L_{ms}) \end{bmatrix} \begin{bmatrix} i_{sq} \\ i_{rq1} \\ i_{rq2} \end{bmatrix}. \tag{3.46}$$

for the q-axis. Lumping Equations (3.45) and (3.46) together, we obtain the following composite flux-current relationships

$$\begin{bmatrix} \lambda_{sd} \\ \lambda_{sq} \\ \lambda_{rd1} \\ \lambda_{rq1} \\ \lambda_{rd2} \\ \lambda_{rq2} \end{bmatrix} = \begin{bmatrix} 2L_s & 0 & \frac{3}{2}L_{ms} & 0 & \frac{3}{2}L_{ms} & 0 \\ 0 & 2L_s & 0 & \frac{3}{2}L_{ms} & 0 & -\frac{3}{2}L_{ms} \\ \frac{3}{2}L_{ms} & 0 & L_r & 0 & 0 & 0 \\ 0 & \frac{3}{2}L_{ms} & 0 & L_r & 0 & 0 \\ \frac{3}{2}L_{ms} & 0 & 0 & 0 & L_r & 0 \\ 0 & -\frac{3}{2}L_{ms} & 0 & 0 & 0 & L_r \end{bmatrix} \begin{bmatrix} i_{sd} \\ i_{sq} \\ i_{rd1} \\ i_{rq1} \\ i_{rd2} \\ i_{rq2} \end{bmatrix} \tag{3.47}$$

where $L_s = (L_{\ell s} + \frac{3}{2}L_{ms})$ and $L_r = (L_{\ell r} + \frac{3}{2}L_{ms})$.

3.1.2 State-Space Form of the Voltage Equations of Two Series-Connected Induction Machines

State-space variables are defined by decomposing each space vector in the previous model into real and imaginary parts. By decomposing $\vec{\lambda}_s$, $\vec{\lambda}_{r1}$, and $\vec{\lambda}_{r2}$, our model will have six flux states. First, Equation (3.24),

$$\vec{v}_s = 2R_s\vec{i}_s + \frac{d\vec{\lambda}_s}{dt} \tag{3.48}$$

is replaced with

$$(v_{sd} + jv_{sq}) = 2R_s(i_{sd} + ji_{sq}) + \frac{d}{dt}(\lambda_{sd} + j\lambda_{sq}) \tag{3.49}$$

yielding two real stator differential equations,

$$\frac{d\lambda_{sd}}{dt} = -2R_s i_{sd} + v_{sd} \tag{3.50}$$

$$\frac{d\lambda_{sq}}{dt} = -2R_s i_{sq} + v_{sq}. \tag{3.51}$$

Similarly, the rotor flux vector equation for machine 1,

$$\frac{d\vec{\lambda}'_{r1}}{dt} = -R_r \vec{i}'_{r1} + j\omega_1 \vec{\lambda}'_{r1} \tag{3.52}$$

is replaced with

$$\frac{d}{dt}(\lambda_{rd1} + j\lambda_{rq1}) = -R_r(i_{d1} + ji_{q1}) + j\omega_1(\lambda_{rd1} + j\lambda_{rq1}) \tag{3.53}$$

yielding the following two real rotor differential equations for machine 1

$$\frac{d\lambda_{rd1}}{dt} = -R_r i_{rd1} - \omega_1 \lambda_{rq1} \tag{3.54}$$

$$\frac{d\lambda_{rq1}}{dt} = -R_r i_{rq1} + \omega_1 \lambda_{rd1}. \tag{3.55}$$

For the second machine, its rotor flux vector equation,

$$\frac{d\vec{\lambda}'_{r2}}{dt} = -R_r \vec{i}'_{r2} + j\omega_2 \vec{\lambda}'_{r2} \tag{3.56}$$

is replaced with

$$\frac{d}{dt}(\lambda_{rd2} + j\lambda_{rq2}) = -R_r(i_{rd2} + ji_{rq2}) + j\omega_2(\lambda_{rd2} + j\lambda_{rq2}) \tag{3.57}$$

yielding the following two real rotor differential equations

$$\frac{d\lambda_{rd2}}{dt} = -R_r i_{rd2} - \omega_2 \lambda_{rq2} \tag{3.58}$$

$$\frac{d\lambda_{rq2}}{dt} = -R_r i_{rq2} + \omega_2 \lambda_{rd2} \tag{3.59}$$

To summarize, the following six voltage equations have been obtained

$$\frac{d\lambda_{sd}}{dt} = -2R_s i_{sd} + v_d \tag{3.60}$$

$$\frac{d\lambda_{sq}}{dt} = -2R_s i_{sq} + v_q \tag{3.61}$$

$$\frac{d\lambda_{rd1}}{dt} = -R_r i_{rd1} - \omega_1 \lambda_{rq1} \tag{3.62}$$

$$\frac{d\lambda_{rq1}}{dt} = -R_r i_{rq1} + \omega_1 \lambda_{rd1} \tag{3.63}$$

$$\frac{d\lambda_{rd2}}{dt} = -R_r i_{rd2} - \omega_2 \lambda_{rq2} \tag{3.64}$$

$$\frac{d\lambda_{rq2}}{dt} = -R_r i_{rq2} + \omega_2 \lambda_{rd2} \tag{3.65}$$

Replacing flux variables in Equations (3.60) to (3.65) by voltage variables and inductances by 60-Hz reactances yields the following equations

$$\frac{1}{\omega_s}\frac{d\Psi_{sd}}{dt} = -2R_s i_{sd} + v_{sd} \tag{3.66}$$

$$\frac{1}{\omega_s}\frac{d\Psi_{sq}}{dt} = -2R_s i_{sq} + v_{sq} \tag{3.67}$$

$$\frac{1}{\omega_s}\frac{d\Psi_{rd1}}{dt} = -R_r i_{rd1} - \frac{\omega_1}{\omega_s}\Psi_{rq1} \tag{3.68}$$

$$\frac{1}{\omega_s}\frac{d\Psi_{rq1}}{dt} = -R_r i_{rq1} + \frac{\omega_1}{\omega_s}\Psi_{rd1} \tag{3.69}$$

$$\frac{1}{\omega_s}\frac{d\Psi_{rd2}}{dt} = -R_r i_{rd2} - \frac{\omega_2}{\omega_s}\Psi_{rq2} \tag{3.70}$$

$$\frac{1}{\omega_s}\frac{d\Psi_{rq2}}{dt} = -R_r i_{rq2} + \frac{\omega_2}{\omega_s}\Psi_{rd2} \tag{3.71}$$

A common reference speed direction ω is chosen so that

$$\omega \;=\; \omega_1 \;=\; \omega_2. \tag{3.72}$$

By substituting this speed relation into Equations (3.66) through (3.71), the following dynamic equations are obtained

$$\begin{aligned}
\frac{1}{\omega_s}\frac{d\Psi_{sd}}{dt} &= -2R_s i_{sd} + v_{sd} && (3.73)\\
\frac{1}{\omega_s}\frac{d\Psi_{sq}}{dt} &= -2R_s i_{sq} + v_{sq} && (3.74)\\
\frac{1}{\omega_s}\frac{d\Psi_{rd1}}{dt} &= -R_r i_{rd1} - \frac{\omega}{\omega_s}\Psi_{rq1} && (3.75)\\
\frac{1}{\omega_s}\frac{d\Psi_{rq1}}{dt} &= -R_r i_{rq1} + \frac{\omega}{\omega_s}\Psi_{rd1} && (3.76)\\
\frac{1}{\omega_s}\frac{d\Psi_{rd2}}{dt} &= -R_r i_{rd2} - \frac{\omega}{\omega_s}\Psi_{rq2} && (3.77)\\
\frac{1}{\omega_s}\frac{d\Psi_{rq2}}{dt} &= -R_r i_{rq2} + \frac{\omega}{\omega_s}\Psi_{rd2}. && (3.78)
\end{aligned}$$

3.1.3 Torque Equation

According to Appendix A, the developed electromagnetic torque in a three-phase induction machine is given by

$$T_e \;=\; \left(\frac{3}{4}\right)\left(\frac{p}{2}\right)\left[\Re_e\left\{j\frac{3}{2}L_{ms}\vec{i}_r e^{j\theta}\vec{i}_s^{\,*} + j\frac{3}{2}L_{ms}e^{-j\theta}\vec{i}_s\vec{i}_r^{\,*}\right\}\right] \tag{3.79}$$

which simplifies to

$$T_e \;=\; \left(\frac{3}{2}M'_{sr}\right)\left(\frac{p}{2}\right)\left(\frac{3}{2}\right)\Im_m\{\vec{i}_s\vec{i}_r^{\,*\prime}\} \tag{3.80}$$

where

$$\vec{i}'_r = \vec{i}_r e^{j\theta} \tag{3.81}$$

is a space vector in the stationary stator reference frame. Recalling Equations (3.33) to (3.35) and decomposing them using real and imaginary components, we get

$$\vec{i}_{s1} = i_{sd1} + ji_{sq1} = \vec{i}_s = i_{sd} + ji_{sq} \tag{3.82}$$

$$\vec{i}^*_{s2} = i_{sd2} - ji_{sq2} = \vec{i}_s = i_{sd} + ji_{sq}. \tag{3.83}$$

Substituting these current components into the torque expression for the first machine yields

$$T_{e1} = \left(\frac{p}{2}\right)\left(\frac{3}{2}L_{ms}\right)\left(\frac{3}{2}\right)\Im_m\{\vec{i}_{s1}\vec{i}'^*_{r1}\} \tag{3.84}$$

$$= \left(\frac{3}{2}L_{ms}\right)\left(\frac{p}{2}\right)\left(\frac{3}{2}\right)\Im_m\{(i_{sd1} + ji_{sq1})(i'_{rd1} - ji'_{rq1})\} \tag{3.85}$$

$$= \left(\frac{3}{2}L_{ms}\right)\left(\frac{p}{2}\right)\left(\frac{3}{2}\right)\Im_m\{(i_{sd} + ji_{sq})(i'_{rd1} - ji'_{rq1})\} \tag{3.86}$$

$$= \left(\frac{3}{2}L_{ms}\right)\left(\frac{p}{2}\right)\left(\frac{3}{2}\right)(i_{sq}i'_{rd1} - i_{sd}i'_{rq1}) \tag{3.87}$$

Similarly, the torque produced by the second machine is given by

$$T_{e2} = \left(\frac{p}{2}\right)\left(\frac{3}{2}L_{ms}\right)\left(\frac{3}{2}\right)\Im_m\{\vec{i}_{s2}\vec{i}'^*_{r2}\} \tag{3.88}$$

$$= \left(\frac{p}{2}\right)\left(\frac{3}{2}L_{ms}\right)\left(\frac{3}{2}\right)\Im_m\{(i_{sd2} + ji_{sq2})(i'_{rd2} - ji'_{rq2})\} \tag{3.89}$$

$$= \left(\frac{p}{2}\right)\left(\frac{3}{2}L_{ms}\right)\left(\frac{3}{2}\right)\Im_m\{(i_{sd} - ji_{sq})(i'_{rd2} - ji'_{rq2})\} \tag{3.90}$$

$$= -\left(\frac{3}{2}L_{ms}\right)\left(\frac{p}{2}\right)\left(\frac{3}{2}\right)(i_{sq}i'_{rd2} + i_{sd}i'_{rq2}). \tag{3.91}$$

Since the two machines are rigidly coupled through the shaft, the aggregate torque equation is given by

$$\frac{J}{(p/2)}\frac{d\omega}{dt} = T_{e1} + T_{e2} - T_m \tag{3.92}$$

where J is the sum of the inertias of both machines and T_m is the applied mechanical torque.

Substituting Equations (3.87) and (3.91) into (3.92) yields the following torque equation

$$\frac{J}{p/2}\frac{d\omega}{dt} = \left(\frac{p}{2}\right)\left(\frac{9L_{ms}}{4}\right)(i_{sq}i'_{rd1} - i_{sd}i'_{rq1} - i_{sq}i'_{rd2} - i_{sd}i'_{rq2}) - T_m \tag{3.93}$$

3.1.4 Three-Phase Induction Machine Model in a Synchronously-Rotating Reference Frame

In this section, the complete model derived in a stationary reference frame is reproduced below using voltage variables as

$$\frac{1}{\omega_s}\frac{d\Psi_{sd}}{dt} = -2R_s i_{sd} + v_{sd} \tag{3.94}$$

$$\frac{1}{\omega_s}\frac{d\Psi_{sq}}{dt} = -2R_s i_{sq} + v_{sq} \tag{3.95}$$

$$\frac{1}{\omega_s}\frac{d\Psi_{rd1}}{dt} = -R_r i_{rd1} - \frac{\omega}{\omega_s}\Psi_{rq1} \tag{3.96}$$

$$\frac{1}{\omega_s}\frac{d\Psi_{rq1}}{dt} = -R_r i_{rq1} + \frac{\omega}{\omega_s}\Psi_{rd1} \tag{3.97}$$

$$\frac{1}{\omega_s}\frac{d\Psi_{rd2}}{dt} = -R_r i_{rd2} - \frac{\omega}{\omega_s}\Psi_{rq2} \tag{3.98}$$

$$\frac{1}{\omega_s}\frac{d\Psi_{rq2}}{dt} = -R_r i_{rq2} + \frac{\omega}{\omega_s}\Psi_{rd2} \tag{3.99}$$

$$\frac{J}{(p/2)}\frac{d\omega}{dt} = \left[\left(\frac{p}{2}\right)\left(\frac{9M_{sr}}{4}\right)[(i_{sq}i'_{rd1} - i_{sd}i'_{rq1}) - (i_{sq}i'_{rd2} + i_{sd}i'_{rq2})] - T_m\right]. \tag{3.100}$$

Since the synchronously-rotating reference frame is a special and useful reference frame for running simulations, the previous model is now transformed to this reference frame using a standard procedure as

$$\frac{1}{\omega_s}\frac{d\Psi_{sd}}{dt} = -2R_s i_{sd} + \Psi_{sq} + v_{sd} \tag{3.101}$$

$$\frac{1}{\omega_s}\frac{d\Psi_{sq}}{dt} = -2R_s i_{sq} - \Psi_{sd} + v_{sq} \tag{3.102}$$

$$\frac{1}{\omega_s}\frac{d\Psi_{rd1}}{dt} = -R_r i_{rd1} - \frac{\omega}{\omega_s}\Psi_{rq1} + \Psi_{rq1} \tag{3.103}$$

$$\frac{1}{\omega_s}\frac{d\Psi_{rq1}}{dt} = -R_r i_{rq1} + \frac{\omega}{\omega_s}\Psi_{rd1} - \Psi_{rd1} \tag{3.104}$$

$$\frac{1}{\omega_s}\frac{d\Psi_{rd2}}{dt} = -R_r i_{rd2} - \frac{\omega}{\omega_s}\Psi_{rq2} - \Psi_{rq2} \tag{3.105}$$

$$\frac{1}{\omega_s}\frac{d\Psi_{rq2}}{dt} = -R_r i_{rq2} + \frac{\omega}{\omega_s}\Psi_{rd2} + \Psi_{rd2} \tag{3.106}$$

$$\frac{J}{(p/2)}\frac{d\omega}{dt} = \left[\left(\frac{p}{2}\right)\left(\frac{9X_{ms}}{4\omega_s}\right)\left[(i_{sq}i'_{rd1} - i_{sd}i'_{rq1}) - (i_{sq}i'_{rd2} + i_{sd}i'_{rq2})\right] - T_m\right] \tag{3.107}$$

where the new variables have kept the same names in both reference frames. After some manipulations, this model simplifies to

$$\frac{1}{\omega_s}\frac{d\Psi_{sd}}{dt} = -2R_s i_{sd} + \Psi_{sq} + v_{sd} \tag{3.108}$$

$$\frac{1}{\omega_s}\frac{d\Psi_{sq}}{dt} = -2R_s i_{sq} - \Psi_{sd} + v_{sq} \tag{3.109}$$

$$\frac{1}{\omega_s}\frac{d\Psi_{rd1}}{dt} = -R_r i_{rd1} + \left(\frac{\omega_s - \omega}{\omega_s}\right)\Psi_{rq1} \tag{3.110}$$

$$\frac{1}{\omega_s}\frac{d\Psi_{rq1}}{dt} = -R_r i_{rq1} - \left(\frac{\omega_s - \omega}{\omega_s}\right)\Psi_{rd1} \tag{3.111}$$

$$\frac{1}{\omega_s}\frac{d\Psi_{rd2}}{dt} = -R_r i_{rd2} - \left(\frac{\omega_s + \omega}{\omega_s}\right)\Psi_{rq2} \tag{3.112}$$

$$\frac{1}{\omega_s}\frac{d\Psi_{rq2}}{dt} = -R_r i_{rq2} + \left(\frac{\omega_s + \omega}{\omega_s}\right)\Psi_{rd2} \tag{3.113}$$

$$\frac{J}{(p/2)}\frac{d\omega}{dt} = \left(\frac{p}{2}\right)\left(\frac{9X_{ms}}{4\omega_s}\right)\left[(i_{sq}i'_{rd1} - i_{sd}i'_{rq1}) - (i_{sq}i'_{rd2} + i_{sd}i'_{rq2})\right] - T_m. \tag{3.114}$$

The flux-current relationships remain as in (4.38), that is

$$\begin{bmatrix} \Psi_{sd} \\ \Psi_{sq} \\ \Psi_{rd1} \\ \Psi_{rq1} \\ \Psi_{rd2} \\ \Psi_{rq2} \end{bmatrix} = \begin{bmatrix} 2X_s & 0 & \frac{3}{2}X_{ms} & 0 & \frac{3}{2}X_{ms} & 0 \\ 0 & 2X_s & 0 & \frac{3}{2}X_{ms} & 0 & -\frac{3}{2}X_{ms} \\ \frac{3}{2}X_{ms} & 0 & X_r & 0 & 0 & 0 \\ 0 & \frac{3}{2}X_{ms} & 0 & X_r & 0 & 0 \\ \frac{3}{2}X_{ms} & 0 & 0 & 0 & X_r & 0 \\ 0 & -\frac{3}{2}X_{ms} & 0 & 0 & 0 & X_r \end{bmatrix} \begin{bmatrix} i_{sd} \\ i_{sq} \\ i_{rd1} \\ i_{rq1} \\ i_{rd2} \\ i_{rq2} \end{bmatrix} \tag{3.115}$$

where $X_s = (X_{\ell s} + \frac{3}{2}X_{ms})$, $X_r = (X_{\ell r} + \frac{3}{2}X_{ms})$, and $X_{ms} = \omega_s L_{ms}$.

CHAPTER 4

MODEL VALIDATION AND SIMULATIONS

4.1 Simulation Results

In this section, the dynamic performance of the models derived in previous chapters is compared. The models simulated in this chapter include the following:

- Exact fourth-order dq model;
- Exact seventh-order dq model;
- Averaged seventh-order dq model;
- Averaged seventh-order fb model;
- Seventh-order model of two three-phase induction machines.

The auxiliary winding of a single-phase induction machine has been neglected in all of these simulations. All models will be simulated with an initial speed condition of 75% of rated speed and with zero initial currents.

A load torque $T_m = 2.5$ N-m is applied at $t = 0.5$ s and removed at $t = 1.5$ s. All models are simulated using classical fourth-order Runge-Kutta method with a uniform step size $\Delta t = 0.1$ ms.

4.1.1 Simulation of Exact Fourth-Order dq Model

Figure 4.1 shows the dynamic speed response of a single-phase induction machine using its original fourth-order model described by Equations (2.33) through (2.35) and (2.37). The following initial conditions are used in this simulation:

$$\begin{bmatrix} \psi_s(0) \\ \psi_d(0) \\ \psi_q(0) \\ \omega(0) \end{bmatrix} = \begin{bmatrix} 0 \\ 0 \\ 0 \\ 0.75\omega_s \end{bmatrix}. \tag{4.1}$$

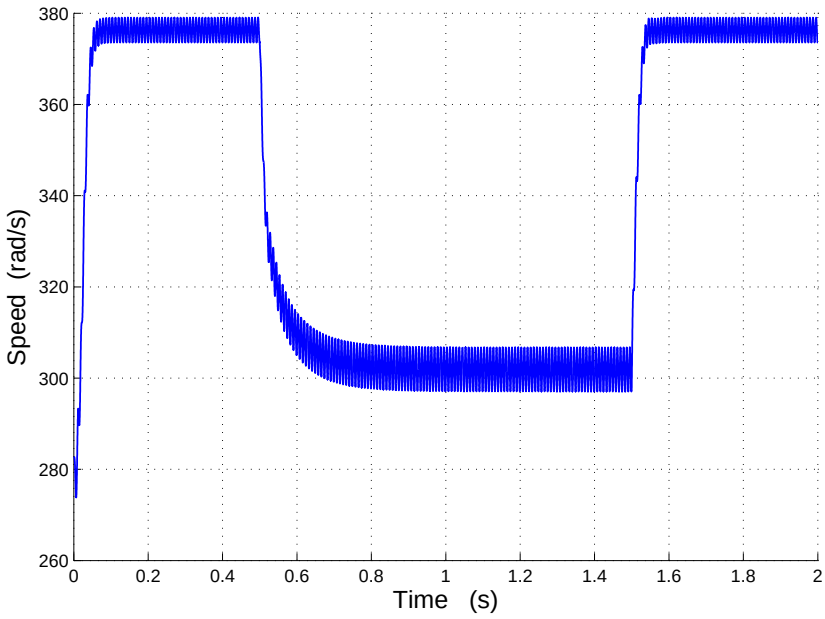

Figure 4.1: Speed Response of Exact Fourth-Order Model

As expected, the steady-state speed pulsates at twice the synchronous frequency for both no-load and loaded conditions. Based on the characteristics of an induction machine, as the machine is loaded at $t = 0.5$ s, the speed of the machines drops to

a lower value and, after removing the load at $t = 1.5$ s, the speed of the machine returns to its no-load steady-state value.

4.1.2 Simulation Comparison of Fourth-Order and Exact Seventh-Order dq Models

To simulate the seventh-order dq-model, the initial conditions used are

$$\begin{bmatrix} \psi_{sx}(0) \\ \psi_{sy}(0) \\ \psi_{dx}(0) \\ \psi_{dy}(0) \\ \psi_{qx}(0) \\ \psi_{qy}(0) \\ \omega(0) \end{bmatrix} = \begin{bmatrix} 0 \\ 0 \\ 0 \\ 0 \\ 0 \\ 0 \\ 0.75\omega_s \end{bmatrix}. \tag{4.2}$$

Figure 4.2 illustrates the speed responses of both the fourth-order and seventh-order models in dq-coordinates. This figure shows that both models yield identical dynamic speed responses verifying the validity of the augmented model.

4.1.3 Simulation Comparison of Fourth-Order and Averaged Seventh-Order dq Models

Equations (2.57) through (2.60) describe the averaged seventh-order model of a single-phase induction machine in dq coordinates. By averaging the double-frequency terms ($e^{j2\omega_s t}$ and $e^{-j2\omega_s t}$) in the exact seventh-order model, a model where the speed is constant in steady state is obtained.

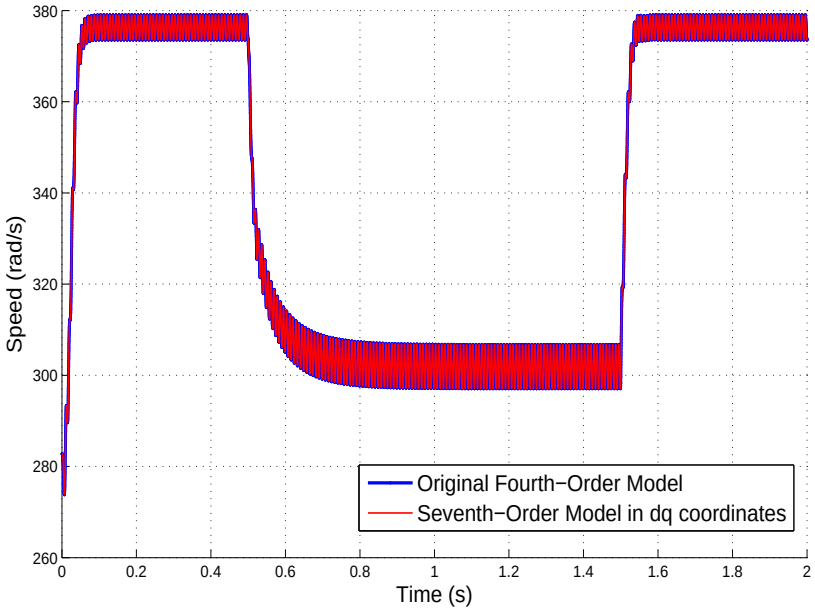

Figure 4.2: Speed Responses of Exact Fourth-Order and Seventh-Order dq Models

Transforming the dq-model to a model with forward and backward components using the defined power-invariant transformation matrices in (2.70) and (2.73) does not change the dynamic speed response that is shown in Figure 4.2.

4.1.4 Simulation Comparison of Fourth-Order and Averaged Seventh-Order fb Models

In this section, we compare the speed responses of the original fourth-order model and the averaged seventh-order fb-model. As expected, the speed of the machine is constant during steady state and without oscillations as shown in Figure 4.3 in the averaged model.

During the initial electrical transient, the speed of the averaged model does not match the exact speed of the original model. The explanation is that the stator

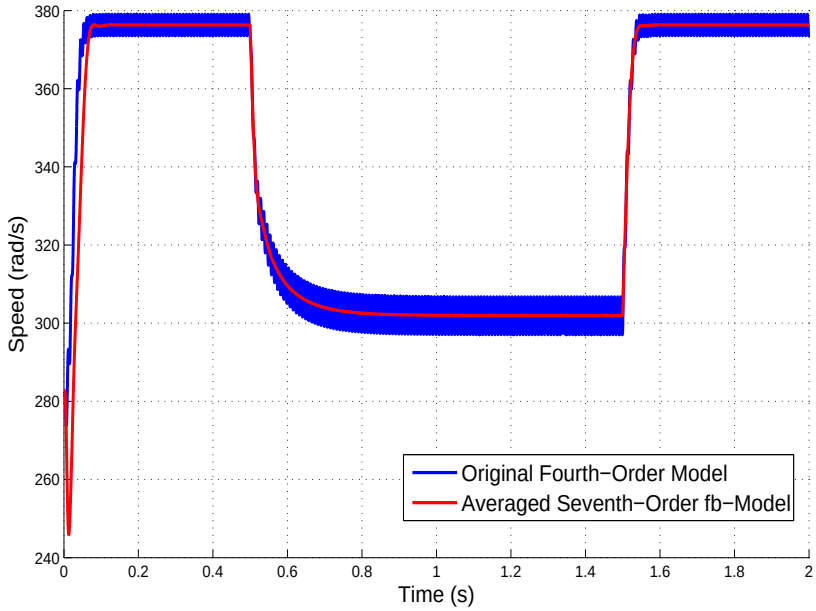

Figure 4.3: Speed Responses of Averaged Seventh-Order fb-Model and Seventh-Order Model of Two Three-Phase Series-Connected Induction Machines

and rotor electrical transients are differently excited in both models. Following the mechanical disturbance at $t = 0\ s$, the stator and rotor electrical transients are not excited and in this model the averaged speed follows the average of the exact pulsating speed.

4.1.5 Simulation Comparison of Averaged Seventh-Order fb-Model and Seventh-Order Model of Two Three-Phase Series-Connected Induction Machines

The simulations of the fb-model of a single-phase induction machine and two three-phase series-connected induction machines yield interesting results. Figure 4.4 clearly shows that both models are superimposed with identical dynamic speed responses during both transient and steady states.

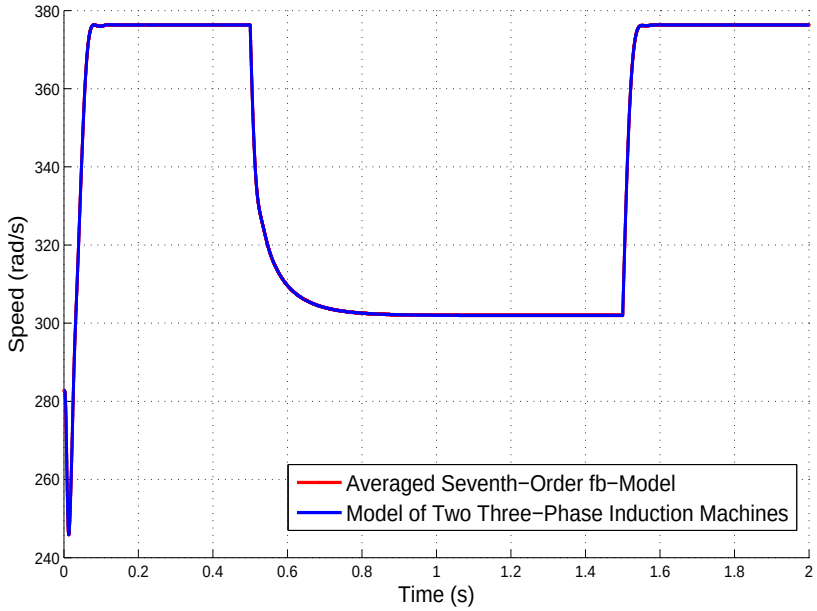

Figure 4.4: Speed Responses of Averaged Seventh-Order fb-Model and Seventh-Order Model of Two Three-Phase Series-Connected Induction Machines

4.2 Applications

In this section, the small-signal stability of the averaged seventh-order fb-model using eigenvalue analysis is studied. At a certain operating speed, the system will become unstable. As will be shown, this instability occurs when one real eigenvalue becomes zero at the maximum pull-out torque.

4.2.1 Eigenvalue Analysis

For a system with n state variables, the eigenvalues of an $n \times n$ matrix A are the n solutions of the characteristic equation

$$p(\lambda) \quad = \quad \det(A - \lambda I) \quad = \quad 0 \tag{4.3}$$

Using the machine parameters in Table 4.2, Equations (2.84) to (2.90) yields a 7×7 system matrix A for the averaged seventh-order fb-model. The maximum torque of

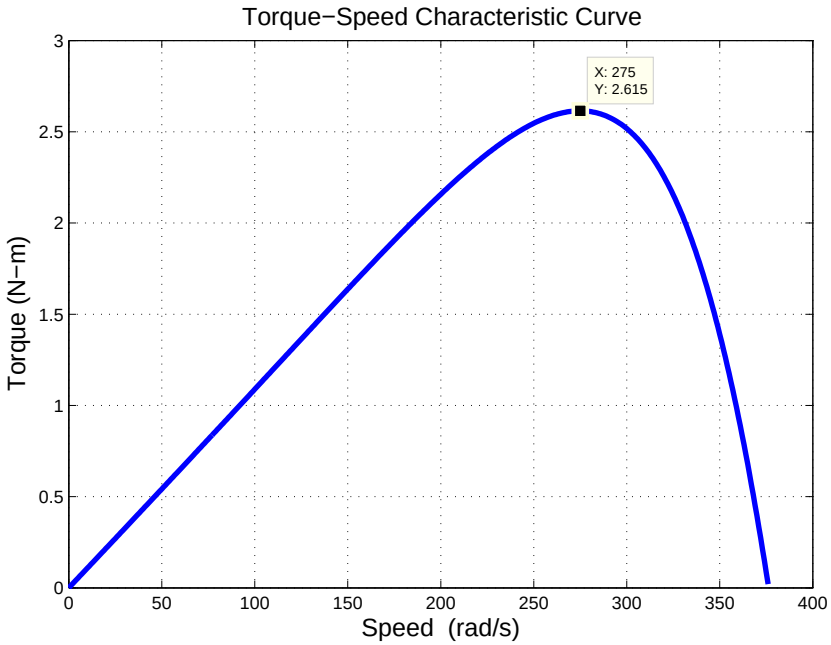

Figure 4.5: Torque-Speed Characteristic Curve for Averaged Seventh-Order fb-Model

about 2.6 (N-m) occurs at an electrical speed of 275 (rad/s) as shown in Figure 4.5. The machine cannot handle additional torque and it is expected that the machine will stall for a torque larger than 2.6 (N-m). This analysis assumes a constant mechanical load torque.

Figure 4.6 shows the real eigenvalue corresponding to each operating speed. At the speed of 275 (rad/s), this eigenvalue becomes zero, verifying the instability of the system at speeds below 275 (rad/s).

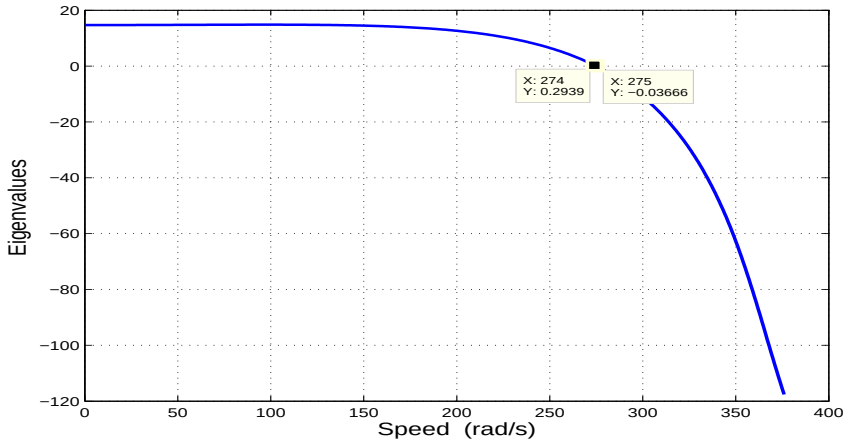

Figure 4.6: Speed-Eigenvalue Curve for Averaged Seventh-Order fb-Model

4.2.2 Participation Factors

In the study of dynamic systems, it may be necessary to construct reduced-order models for dynamic stability studies by retaining only a few modes of interest. It then becomes important to determine which state variables significantly participate in the selected modes.

Verghese et al. [9] proposed a tool known as a participation factor to calculate a dimensionless measure of how much each state variable contributes to a given mode. Given a linear system

$$\dot{x} \quad = \quad Ax \tag{4.4}$$

the participation factor is defined as

$$p_{ki} \quad = \quad \frac{w_{ki} v_{ki}}{w_i^t v_i} \tag{4.5}$$

where w_{ki} and v_{ki} are the k^{th} entries in the left and right eigenvectors associated with the i^{th} eigenvalue. The normalization of the left and right eigenvectors yields

$$w_i^t v_i \quad = \quad \sum_{k=1}^{n} p_{ki} \quad = \quad 1. \tag{4.6}$$

In order to obtain these participation factors for the sole real mode, the seventh-order fb-model is linearized for a defined speed range from 0 to ω_s. For example, the participation factors at $\omega = 350$ (rad/s) are

$$(p_{k7})^T \quad = \quad \begin{bmatrix} -0.224 & 0.014 & -0.263 & 0.294 & -0.007 & 0.008 & 0.977 \end{bmatrix} \tag{4.7}$$

indicating that Ψ_{sy}, Ψ_{fy}, and ω are the dominant variables in this real mode.

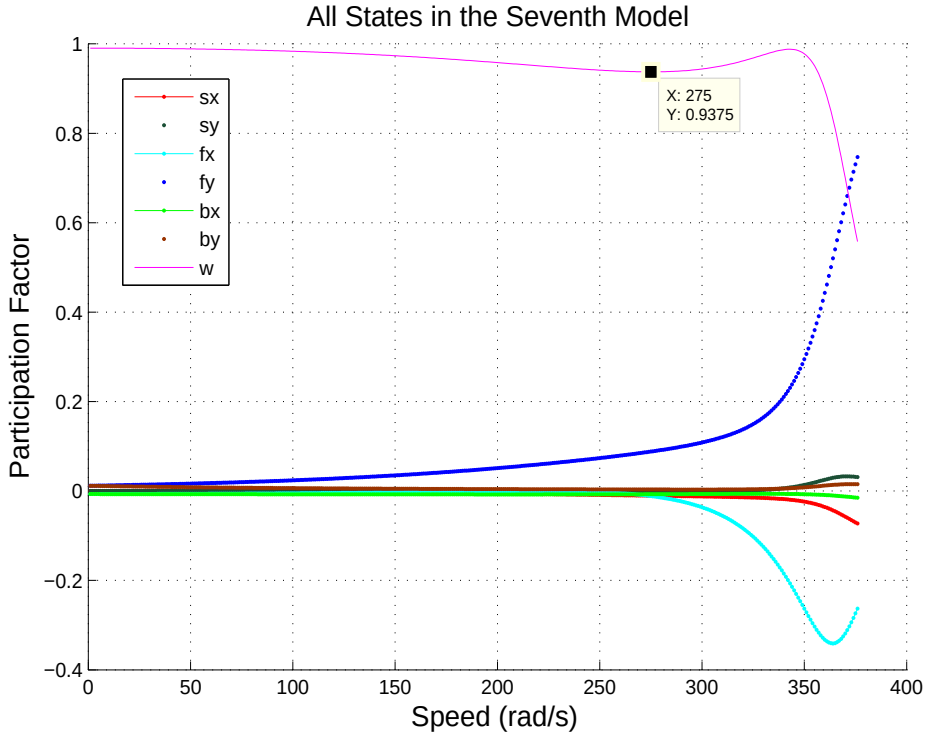

Figure 4.7: Participation Factors of the Seven States in the Real Eigenvalue Mode

As shown in Figure 4.7, the seventh speed state has a large participation factor at all operating points and, at $\omega = 275$ (rad/s), it reaches its lowest value in that

region. It is also interesting that at $\omega = 275$ (rad/s) the machine becomes unstable.

Using a participation factor analysis where p_{77} has a greater value compared to the other states, the slowest state corresponding to the dominant eigenvalue is determined as the speed of the machine. This suggests that the stator and rotor electrical transients are much faster than the rotor speed. Eliminating these fast electrical variables by using a quasi-steady circuit model, a first-order speed model of the machine can be derived. By setting the left-hand sides of the stator and rotor electrical transients to zero, the averaged fb-model in (2.62) to (2.68) becomes

$$0 = -R_s I_{sx} + \Psi_{sy} + V_{sd} \tag{4.8}$$

$$0 = -R_s I_{sy} - \Psi_{sx} + V_{sq} \tag{4.9}$$

$$0 = -\frac{R_r}{2} I_{fx} + \left(\frac{\omega_s - \omega}{\omega_s}\right) \Psi_{fy} \tag{4.10}$$

$$0 = -\frac{R_r}{2} I_{fy} - \left(\frac{\omega_s - \omega}{\omega_s}\right) \Psi_{fx} \tag{4.11}$$

$$0 = -\frac{R_r}{2} I_{bx} + \left(\frac{\omega_s + \omega}{\omega_s}\right) \Psi_{by} \tag{4.12}$$

$$0 = -\frac{R_r}{2} I_{by} - \left(\frac{\omega_s + \omega}{\omega_s}\right) \Psi_{bx} \tag{4.13}$$

$$\frac{J}{(p/2)} \frac{d\omega}{dt} = -\left(\frac{p}{2}\right)\left(\frac{X_{ms}}{\omega_s}\right)\left(\frac{1}{2}\right)[I_{sx}I_{fy} - I_{sy}I_{fx} + I_{sy}I_{bx} - I_{sx}I_{by}] - T_m. \tag{4.14}$$

After solving the above equations, the first-order speed model is

$$\frac{J}{(p/2)} \frac{d\omega}{dt} = -\left(\frac{p}{2}\right)\left(\frac{X_{ms}}{\omega_s}\right)\left(\frac{1}{2}\right)[I_{sx}I_{fy} - I_{sy}I_{fx} + I_{sy}I_{bx} - I_{sx}I_{by}] - T_m \tag{4.15}$$

where the currents in (4.8) - (4.13) are solved in terms of speed, ω, using

$$\begin{bmatrix} -V_{sd} \\ -V_{sq} \\ 0 \\ 0 \\ 0 \\ 0 \end{bmatrix} = \begin{bmatrix} -R_s & X_s & 0 & \frac{X_{ms}}{2} & 0 & \frac{X_{ms}}{2} \\ -X_s & -R_s & -\frac{X_{ms}}{2} & 0 & -\frac{X_{ms}}{2} & 0 \\ 0 & s\frac{X_{ms}}{2} & -\frac{R_r}{2} & s\frac{X_r}{2} & 0 & 0 \\ -s\frac{X_{ms}}{2} & 0 & -s\frac{X_r}{2} & -\frac{R_r}{2} & 0 & 0 \\ 0 & (2-s)\frac{X_{ms}}{2} & 0 & 0 & -\frac{R_r}{2} & (2-s)\frac{X_r}{2} \\ -(2-s)\frac{X_{ms}}{2} & 0 & 0 & 0 & -(2-s) & -\frac{R_r}{2} \end{bmatrix} \begin{bmatrix} I_{sx} \\ I_{sy} \\ I_{fx} \\ I_{fy} \\ I_{bx} \\ I_{by} \end{bmatrix} \tag{4.16}$$

where $s = (\omega_s - \omega)/\omega_s$ is the slip. Simulating the above model and comparing it with the averaged seventh-order fb-model yields the graph shown in Figure 4.8.

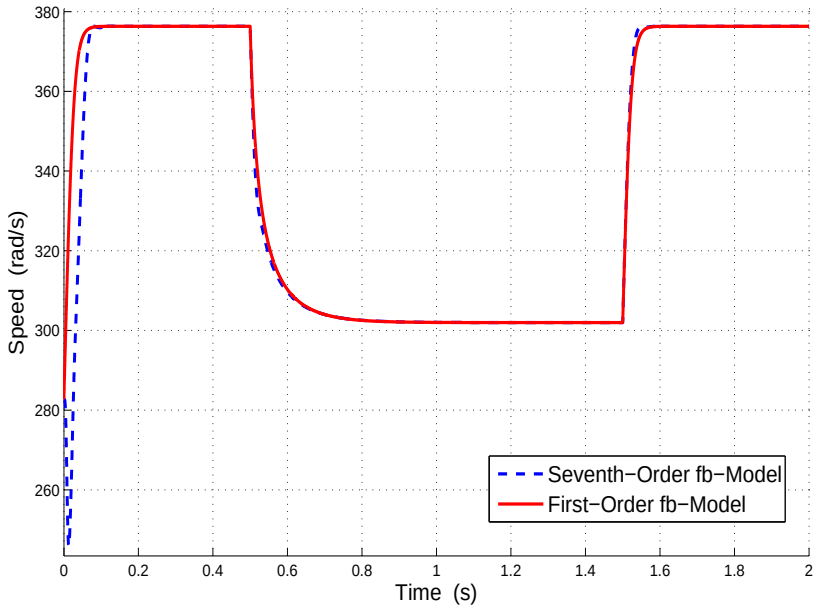

Figure 4.8: Speed Respond of Seventh-Order and First-Order fb-Models

As shown in Figure 4.8, the dynamical speed response of the first-order model follows closely the speed of the seventh-order model after the mechanical disturbance

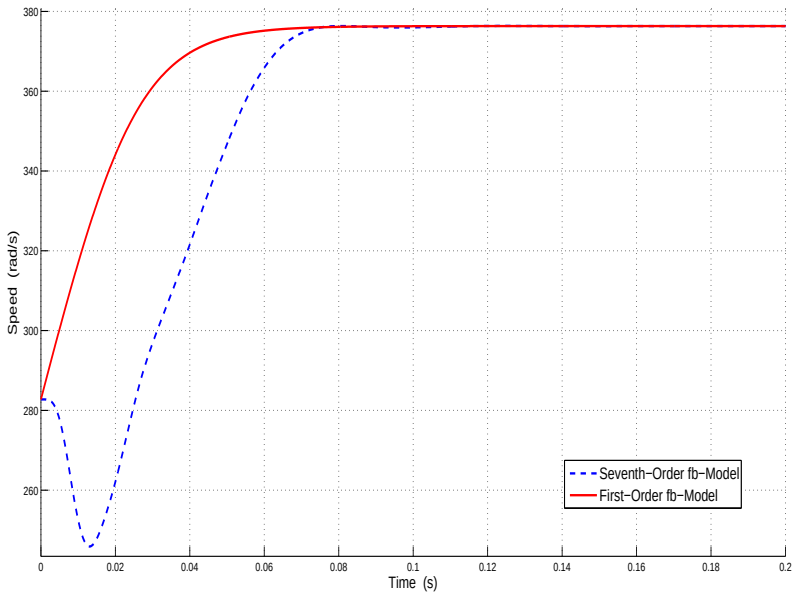

Figure 4.9: Speed Responses of Seventh-Order and First-Order fb-Models During Start-Up

at $t = 0.5$ s. In other words, they are almost identical when the rotor and stator transients are not excited. Since the simulation started with the stator and rotor transients excited, there will be some discrepancies during the initial transient period. By zooming in the time interval of $[0s, 0.2s]$, these discrepancies become more distinguishable as shown in Figure 4.9.

Both models have been simulated with zero initial conditions for the stator and rotor currents. In other words, the electrical transients are simulated as if they were excited since their values differ from their quasi-steady-state circuit values. Using the steady-state circuit in Figure 2.4, it is possible to find the initial current conditions that do not excite the stator and rotor electrical variables. For a slip $s = (1 - 0.75\omega_s/\omega_s) = 0.25$, it is found that the initial stator and rotor flux linkages should be

$$\begin{bmatrix} \psi_{sx}(0) \\ \psi_{sy}(0) \\ \psi_{dx}(0) \\ \psi_{dy}(0) \\ \psi_{qx}(0) \\ \psi_{qy}(0) \\ \omega(0) \end{bmatrix} = \begin{bmatrix} 9.8503 \\ -96.6142 \\ -28.0604 \\ -75.4346 \\ -57.6281 \\ 17.600 \\ 0.75\omega_s \end{bmatrix}. \tag{4.17}$$

Simulating both the first-order and seventh-order models using these initial conditions improves the speed response during the transient state.

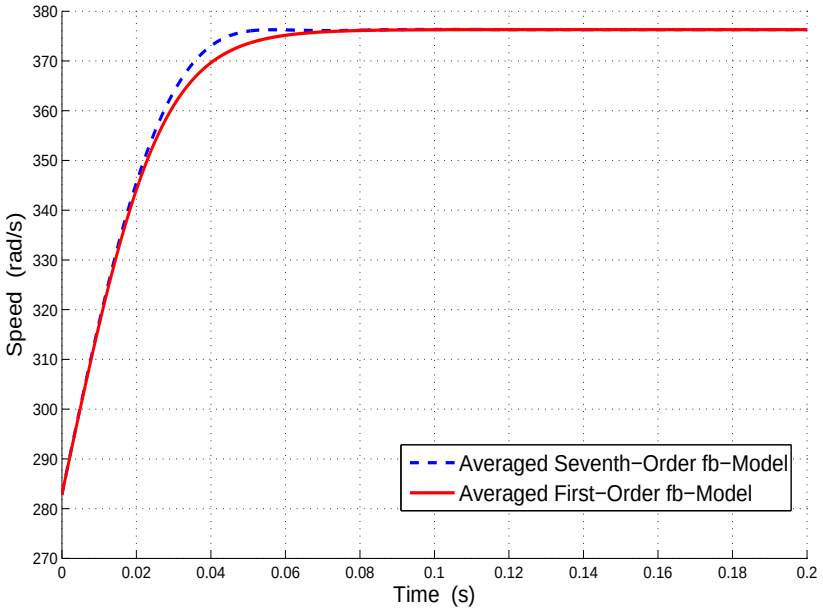

Figure 4.10: Speed Responses of Seventh-Order and First-Order fb-Models with Stator and Rotor Electrical Transients Not Excited

4.2.3 Critical Torque

In this section, the critical torque that can suddenly be applied to a machine at no load is found. The critical torque is the maximum mechanical torque that a machine can handle without stalling. By trial and error, several mechanical load torques are applied until the machine stalls. The case studies will be in the following order:

- Critical torque for original fourth-order
- Critical torque for exact seventh-order dq-model
- Critical torque for averaged seventh-order dq-model and fb-model
- Critical torque for first-order fb-model.

Figure 4.11 shows how the machines will stall for different load torques. Having

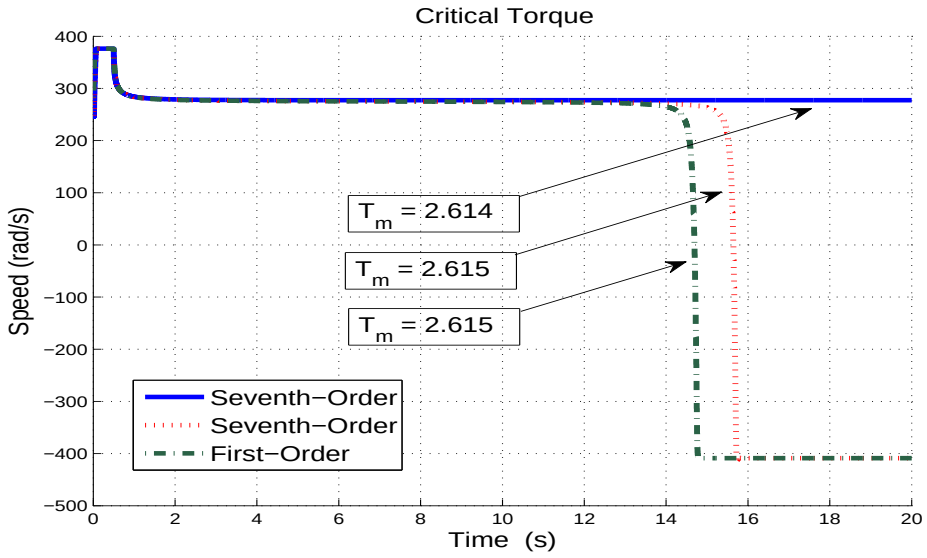

Figure 4.11: Critical Torque Determination Using Several Models

simulated the remaining models, Table 4.1 shows the results for each model.

Table 4.1: Values of Critical Torque for Each Model

Models	Critical Torque (N-m)
Original Fourth−Order	2.612
Seventh−Order dq−Model	2.612
Averaged Seventh−Order dq−Model	2.614
Seventh−Order fb−Model	2.612
Averaged Seventh−Order fb−Model	2.614
First−Order	2.614
TPIM	2.614

From this table, it is obvious that all models become unstable for the same critical load torque of about 2.61 (N-m) as the original fourth-order model does.

4.2.4 Recovering Torque and Speed Pulsations from the Averaged Model

In this section, it is shown how the double-frequency torque and speed oscillations can be recovered using the averaged model. This procedure gives a profound understanding of how a single-phase induction machine behaves.

The stator currents of the exact seventh-order dq-model are first plotted as shown in Figure 4.12.

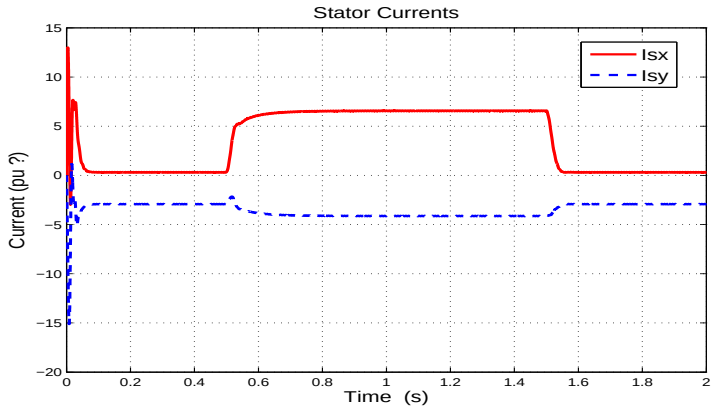

Figure 4.12: Exact Stator Currents I_{sx} and I_{sy} from the Exact Seventh-Order dq-Model

By zooming in the time interval of $[1.45s, 2s]$, Figure 4.13 illustrates the negligible ripples in the stator currents.

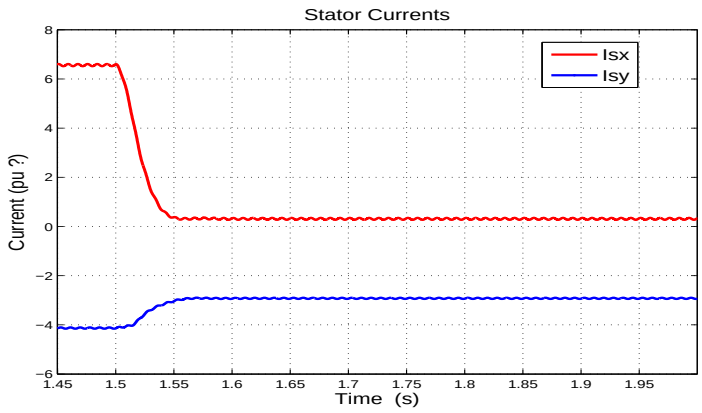

Figure 4.13: Exact Stator Currents I_{sx} and I_{sy} from the Exact Seventh-Order dq-Model

As the ripples or oscillations in these currents are already small, we surmise that the averaging process will eliminate these oscillations in the averaged model. Assuming that these currents are constant, we infer that the speed pulsations can be simply recovered by integrating the double-frequency torque components that were discarded in the averaging process. The averaged current variables obtained in the averaged seventh-order in lieu of the exact current variables are used since they differ by a small oscillatory component.

To integrate and recover the speed oscillations, an eighth differential equation is added to the model with an additional variable denoted as ω_2. It is important, however, to mention that this added differential equation is not part of the model. In other words, it is only used after we have integrated the averaged seventh-order model and found its solutions for the averaged currents. Recalling Equation (2.56),

$$\frac{J}{(p/2)}\frac{d\omega}{dt} = -\left(\frac{1}{2}\right)\left(\frac{p}{2}\right)\left(\frac{X_m}{\omega_s}\right)[I_s I_q^* + I_s^* I_q + I_s I_q e^{j2\omega_s t} + I_s^* I_q^* e^{-j2\omega_s t}] - T_m \tag{4.18}$$

this differential equation is separated into two differential equations as shown below

$$\frac{J}{(p/2)}\frac{d\omega_1}{dt} = -\left(\frac{1}{2}\right)\left(\frac{p}{2}\right)\left(\frac{X_m}{\omega_s}\right)[I_s I_q^* + I_s^* I_q] - T_m \tag{4.19}$$

$$\frac{J}{(p/2)}\frac{d\omega_2}{dt} = -\left(\frac{1}{2}\right)\left(\frac{p}{2}\right)\left(\frac{X_m}{\omega_s}\right)[I_s I_q e^{j2\omega_s t} + I_s^* I_q^* e^{-j2\omega_s t}] \tag{4.20}$$

where ω_1 represents the averaged speed and ω_2 represents the double-frequency oscillations of the speed. Expanding Equations (4.19) and (4.20) yields

$$\frac{J}{(p/2)}\frac{d\omega_1}{dt} = -\left(\frac{1}{2}\right)\left(\frac{p}{2}\right)\left(\frac{X_m}{\omega_s}\right)[I_{sx} I_{qx} + I_{sy} I_{qy}] - T_m \tag{4.21}$$

$$\frac{J}{(p/2)}\frac{d\omega_2}{dt} = -\left(\frac{1}{2}\right)\left(\frac{p}{2}\right)\left(\frac{X_m}{\omega_s}\right)[(I_{sx} I_{qx} - I_{sy} I_{qy})\cos 2\omega_s t - (I_{sx} I_{qy} + I_{sy} I_{qx})\sin 2\omega_s t]. \tag{4.22}$$

The initial conditions for the seven state variables have been obtained from the quasi-steady-state circuit at 75% of synchronous speed. Since one differential equation, the eighth equation, is used to recover the double-frequency oscillations, it should have an appropriate initial condition. The initial condition for the eighth differential equation is obtained by integrating both sides of Equation (4.22) and setting time $t = 0$ s yielding

$$\omega_2(0) = -\left(\frac{1}{J}\right)\left(\frac{p}{2}\right)\left(\frac{1}{2}\right)\left(\frac{p}{2}\right)\left(\frac{X_m}{\omega_s}\right)[(I_{sx}(0) I_{qy}(0) + I_{sy}(0) I_{qx}(0))\frac{\cos 2\omega_s(0)}{2\omega_s}] \tag{4.23}$$

which is equal to -3.8660. The eighth-order model will be simulated using the following

corrected initial conditions for ω_1, and ω_2:

$$\begin{bmatrix} \psi_{sx}(0) \\ \psi_{sy}(0) \\ \psi_{dx}(0) \\ \psi_{dy}(0) \\ \psi_{qx}(0) \\ \psi_{qy}(0) \\ \omega_1(0) \\ \omega_2(0) \end{bmatrix} = \begin{bmatrix} 9.8503 \\ -96.6142 \\ -28.0604 \\ -75.4346 \\ -57.6281 \\ 17.600 \\ 0.75\omega_s + 3.8660 \\ -3.8660 \end{bmatrix}. \tag{4.24}$$

After adding ω_1 and ω_2 together, an almost exact dynamic speed response is obtained as shown in Figure 4.14.

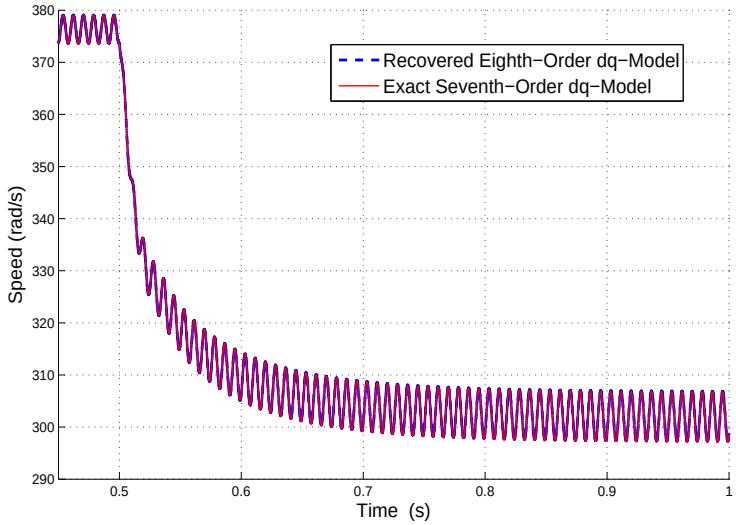

Figure 4.14: Recovering Speed Oscillations

4.2.5 Physical Interpretation

The oscillations from the eighth-order model match perfectly those in the original fourth-order model. It is important to note that the obtained averaged speed and oscillations are added together to get a complete speed response similar to the speed of the fourth-order model.

The following paragraphs explain how these pulsations arise in the single-phase induction machine.

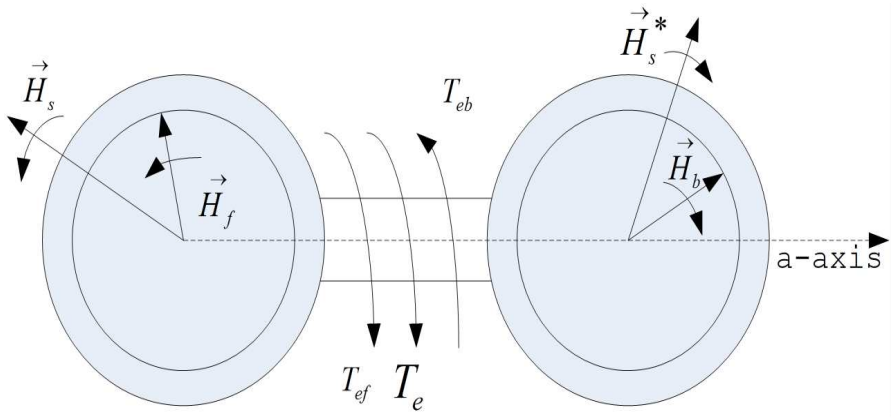

Figure 4.15: Magnetic Fields of Motor and Generator

In Figure 4.15, $\vec{H}_s$ is the stator magnetic field leading the induced forward-rotating rotor magnetic field $\vec{H}_f$ in the left machine. In the right machine, $\vec{H}_s^*$ is the stator magnetic field lagging the induced backward-rotating rotor magnetic field $\vec{H}_b$.

The corresponding stator and rotor magnetic fields in one machine do not interact with those in the other machine. Each three-phase machine will therefore produce a steady torque (forward or backward) on the shaft.

By merging both machines into one solid machine, these four magnetic fields are now located in a common air gap. As shown in Figure 4.16, these four magnetic fields interact with each other and produce double-frequency pulsations in addition to the original two steady torque (forward and backward) components.

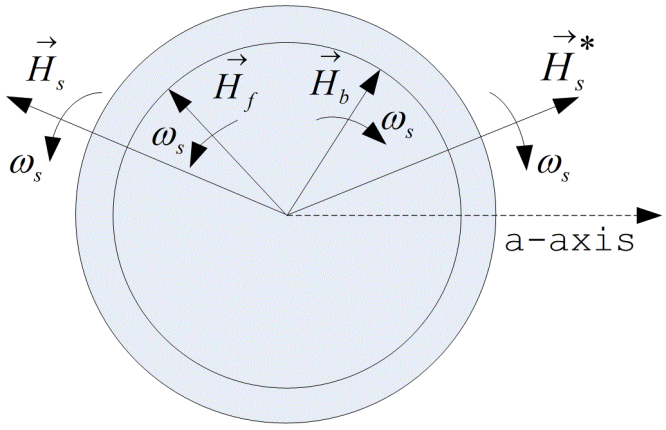

Figure 4.16: Magnetic Fields of the Single-Phase Induction Machine

These interactions can be recovered using Equation (4.22). Since it was possible to recover almost exactly the torque and speed oscillations in a single-phase induction machine, we conclude that these formulas quantify the interactions between the magnetic fields revolving past each other at twice the synchronous speed.

4.3 Parameters

This section provides the parameters of a single-phase induction machine equivalent to those of two three-phase series-connected induction machines. These parameters have been used to simulate the models derived in the previous chapters. There are two different sets of parameters values to simulate the single-phase induction machine and the two three-phase induction machines.

It is shown in Figure 4.4 that the averaged model of a single-phase induction machine and two three-phase series-connected induction machines are identical and have the same dynamic response at both no load and loaded conditions. The parameters of this new setup have been adjusted by aggregating three single-phase induction machines coupled on the same shaft. Figure 4.17 shows how these three single-phase induction machines are connected. To clarify the notation, 1ϕ and 3ϕ will be used to represent, respectively, the parameters of a single-phase machine and each of two three-phase induction machine connected in series.

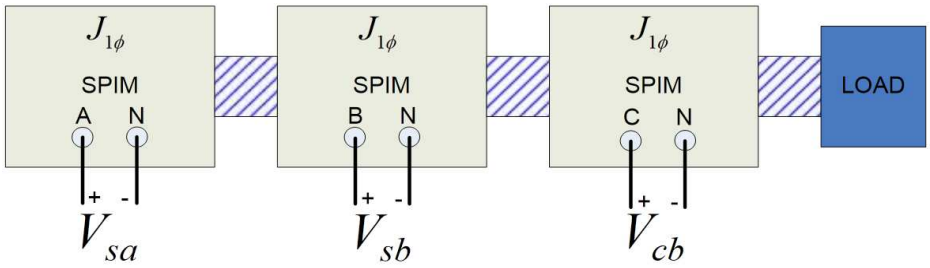

Figure 4.17: Three Single-Phase Induction Machines Coupled on the Same Shaft

In Figure 4.17, $J_{1\phi}$ represents the inertia of a single-phase induction machine. Each of the induction machines above has an equivalent circuit, which is shown in Figure 4.18. The forward component of the single-phase induction machine is highlighted by box M. On the other hand, box N shows the total backward components of three single-phase induction machines rigidly coupled on the same shaft.

The parameters of this representation of three single-phase induction machines are compared to the parameters of two three-phase induction machines, as shown in Figure 3.1.

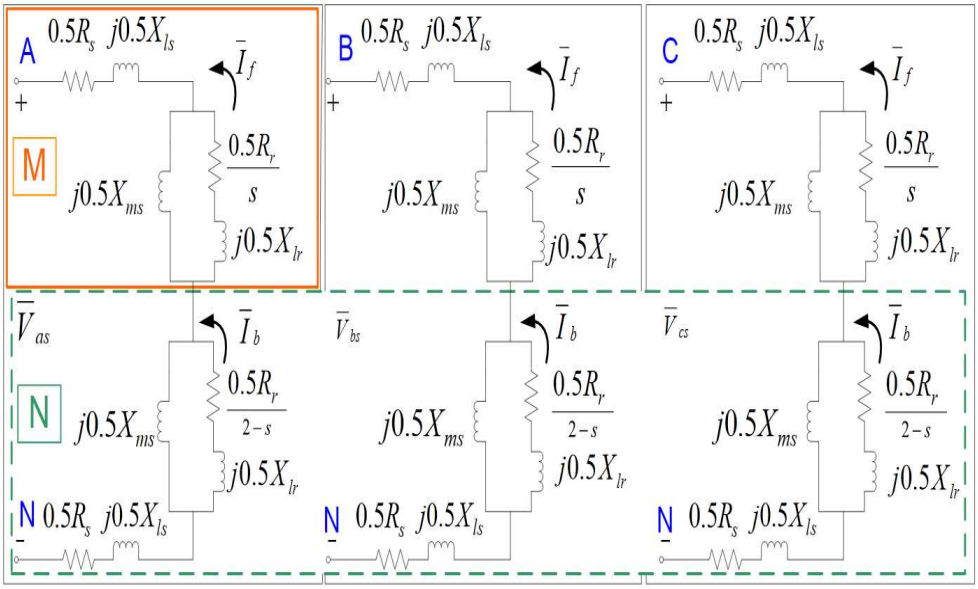

Figure 4.18: Three Quasi-Steady-State Circuits of a Single-Phase Induction Machine

In two three-phase induction machine connected in series, the left machine acts as a forward-torque producing machine and the right machine acts as a backward-torque producing machine.

Figure 4.19(a) simply shows a three-phase induction machine where its circuit is compared with the circuit for single-phase induction machine. The inertia constant of each three-phase machine is represented by $J_{3\phi}$. Therefore, the total inertia constant of both three-phase machines is $2J_{3\phi}$.

By comparing the circuits of both machines, the following relationships are obtained for the stator and rotor resistances,

$$R_{s,3\phi} = \frac{R_{s,1\phi}}{2} \tag{4.25}$$

$$R_{r,3\phi} = \frac{R_{r,1\phi}}{2} \tag{4.26}$$

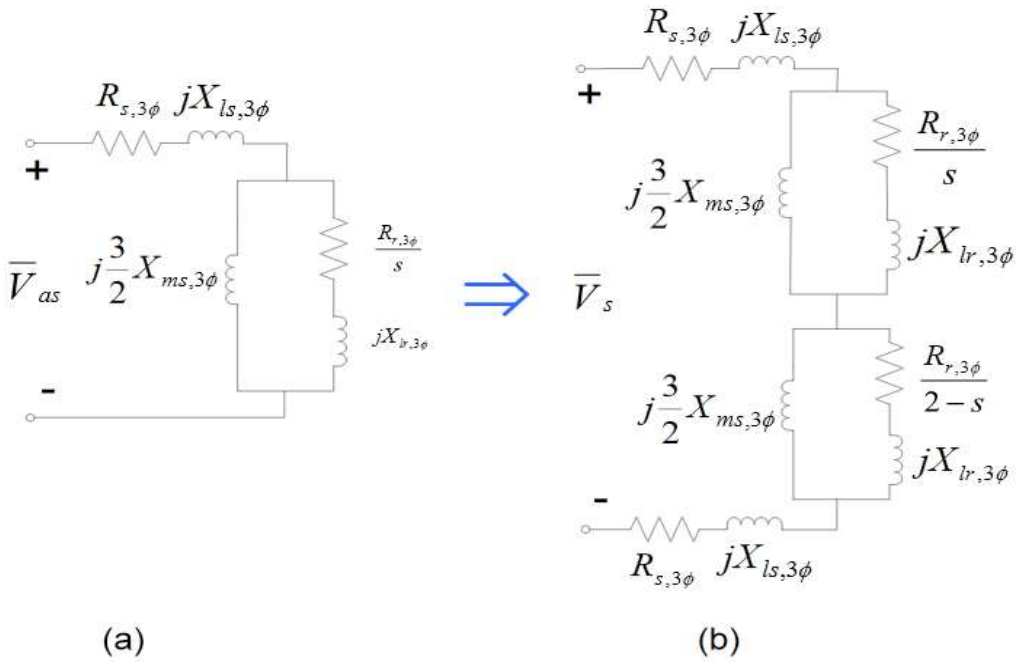

Figure 4.19: (a) Circuit of Three-Phase Induction Machine (b) Circuit of a Two Three-Phase Induction Machines Connected in Series with Opposite Stator Phase Sequences

and for the moment of inertia,

$$2J_{3\phi} = 3J_{1\phi}. \tag{4.27}$$

The leakage reactances are also identified as

$$X_{\ell s,3\phi} = \frac{X_{\ell s,1\phi}}{2} \tag{4.28}$$

$$X_{\ell r,3\phi} = \frac{X_{\ell r,1\phi}}{2} \tag{4.29}$$

and the magnetizing reactance is obtained as

$$X_{ms,3\phi} = \frac{X_{ms,1\phi}}{3}. \tag{4.30}$$

The illustrated results for the single-phase machine have been simulated with numerical example of a 1/4 horse power machine from [10] (page 438) with a peak source voltage of $110\sqrt{2}$ V. The values of the parameters such as resistances, inductances, and moment of inertia are given in Table 4.2.

The terms SPIM and TPIM used in Table 4.2 represent the single-phase induction machine and each of the two three-phase induction machines (TPIM) connected in series.

Table 4.2: Parameters of Each Single-Phase and Three-Phase Induction Machines

Parameter Type	SPIM	TPIM
R_s	2.02	1.01
R_r	4.12	2.06
X_{ms}	66.8	(1/3)66.8/2
X_s	2.79+X_m	2.79+(3/2)X_m
X_r	2.12+X_m	2.12+(3/2)X_m
J	0.00146	3(0.00146)/2
P	4	4

In the final model (3.108) through (3.114), inertias of both machines are added together. The final model for the two three-phase series-connected induction machines is

$$\frac{1}{\omega_s}\frac{d\Psi_{sd}}{dt} = -2R_{s,3\phi}i_{sd} + \Psi_{sq} + v_d \tag{4.31}$$

$$\frac{1}{\omega_s}\frac{d\Psi_{sq}}{dt} = -2R_{s,3\phi}i_{sq} - \Psi_{sd} + v_q \tag{4.32}$$

$$\frac{1}{\omega_s}\frac{d\Psi_{rd1}}{dt} = -R_{r,3\phi}i_{rd1} + \left(\frac{\omega_s - \omega}{\omega_s}\right)\Psi_{rq1} \tag{4.33}$$

$$\frac{1}{\omega_s}\frac{d\Psi_{rq1}}{dt} = -R_{r,3\phi}i_{rq1} - \left(\frac{\omega_s - \omega}{\omega_s}\right)\Psi_{rd1} \tag{4.34}$$

$$\frac{1}{\omega_s}\frac{d\Psi_{rd2}}{dt} = -R_{r,3\phi}i_{rd2} - \left(\frac{\omega_s + \omega}{\omega_s}\right)\Psi_{rq2} \tag{4.35}$$

$$\frac{1}{\omega_s}\frac{d\Psi_{rq2}}{dt} = -R_{r,3\phi}i_{rq2} + \left(\frac{\omega_s + \omega}{\omega_s}\right)\Psi_{rd2} \tag{4.36}$$

$$\frac{2J_{3\phi}}{(p/2)}\frac{d\omega}{dt} = \left(\frac{p}{2}\right)\left(\frac{3}{2}\right)\left(\frac{3X_{ms,3\phi}}{2\omega_s}\right)[(i_{sq}i'_{rd1} - i_{sd}i'_{rq1}) - (i_{sq}i'_{rd2} + i_{sd}i'_{rq2})] - T_m \tag{4.37}$$

with the following flux-current relationships

$$\begin{bmatrix} \Psi_{sd} \\ \Psi_{sq} \\ \Psi_{rd1} \\ \Psi_{rq1} \\ \Psi_{rd2} \\ \Psi_{rq2} \end{bmatrix} = \begin{bmatrix} 2X_{s,3\phi} & 0 & \frac{3}{2}X_{ms,3\phi} & 0 & \frac{3}{2}X_{ms,3\phi} & 0 \\ 0 & 2X_{s,3\phi} & 0 & \frac{3}{2}X_{ms,3\phi} & 0 & -\frac{3}{2}X_{ms,3\phi} \\ \frac{3}{2}X_{ms,3\phi} & 0 & X_{r,3\phi} & 0 & 0 & 0 \\ 0 & \frac{3}{2}X_{ms,3\phi} & 0 & X_{r,3\phi} & 0 & 0 \\ \frac{3}{2}X_{ms,3\phi} & 0 & 0 & 0 & X_{r,3\phi} & 0 \\ 0 & -\frac{3}{2}X_{ms,3\phi} & 0 & 0 & 0 & X_{r,3\phi} \end{bmatrix} \begin{bmatrix} i_{sd} \\ i_{sq} \\ i_{rd1} \\ i_{rq1} \\ i_{rd2} \\ i_{rq2} \end{bmatrix} \tag{4.38}$$

where $X_{s,3\phi} = (X_{\ell s,3\phi} + \frac{3}{2}X_{ms,3\phi})$, $X_{r,3\phi} = (X_{\ell r,3\phi} + \frac{3}{2}X_{ms,3\phi})$, and $X_{ms,3\phi} = \omega_s L_{ms,3\phi}$.

4.4 Experimental Validation

This section gives the results of an experiment verifying the behavior of two three-phase series-connected induction machines. As explained, the net produced torque at standstill is zero for both setups. The machine shaft did not rotate after powering the setup of Figure 4.20, which illustrates how the three-phase induction machines are connected.

Figure 4.20: Two Three-Phase Induction Machine Connected in Series

After powering this setup, the experiment showed that none of the shafts rotated and both shafts remained fixed. Manually turning the shaft in either the forward or backward direction caused both shafts to rotate in the applied torque direction. The setup exhibited this behavior in both directions.

CHAPTER 5

CONCLUSION AND RECOMMENDATIONS

5.1 Conclusion

In this thesis, a seventh-order dq-model of a single-phase induction machine has been developed by postulating the existence of current and flux solutions in a certain form in the original model. This seventh-order dq-model has the exact dynamical behavior as the original fourth-order dq-model.

There are double-frequency terms in the torque equation that cause the single-phase induction machine to have oscillations in its speed. These oscillations can be eliminated by applying standard averaging theory yielding an averaged seventh-order dq-model. Applying an additional transformation using forward and backward components yields a seventh-order fb-model and the standard steady-state equivalent circuit of a single-phase induction machine.

Using space vector theory, a new model for two three-phase induction machines connected in series has been derived. Interestingly, this new model is dynamically equivalent to the averaged model of a seventh-order fb-model single-phase induction machines. This is a new proof of the well-known theory in [4] that supports that two three-phase induction machines connected in series have the same dynamic response

as a single-phase induction machine.

Finally, it has been proved that the double-frequency terms can be recovered using the solution of the averaged model. This recovery is done by assuming that the stator and rotor electrical transients are on their quasi-steady-state manifolds. Appropriate initial conditions have to be determined using the quasi-steady-state circuit. The speed pulsation recovery explains the fact that, in a single-phase machine, the torque and speed vibrations are due to the interaction of the magnetic fields located in the same air gap.

5.2 Recommendations for Future Work

This new model of a single-phase induction machine will be useful in modeling single-phase motor loads in power system stability studies. The dynamic behavior of a single-phase induction machine can be predicted and simulated by using a first-order speed model.

The torque equation of this new model for the single-phase induction machines can be extended to account for the vibrational torques, which include not only the averaged torque but also the double-frequency components and other negligible harmonics. The effect of the vibration on the emitted acoustical noise can be investigated as well as the improvements in the structural design of single-phase induction machines.

In the case of two three-phase induction machines connected in series, the satura-

tion level of rotor or stator windings can also be studied with the help of this model. It is not clear at this point how saturation effects the single-phase machine where all the magnetic fields are present in the same air gap.

REFERENCES

[1] CIGRE Task Force 38.02.05,"Load Modeling and Dynamics," *Electra*, pp. 122-41, May 1990.

[2] S. Ahmed-Zaid (Editor). *Modeling of Single-Phase Induction Motor Loads in Power System Studies*. Electric Power Research Institute, EPRI Report TR-105341, January 1996.

[3] IEEE Task Force on Load Representation for Dynamic Performance, "Load Representation for Dynamic Performance Analysis," *IEEE Transactions on Power Systems*, vol. 8, no. 2, pp. 472-482, May 1993.

[4] P.L. Alger. "The dilemma of Single-Phase Induction Motor Theory." *Power Apparatus and systems, Part III. Transactions of the American Institute of Electrical Engineers*, vol. 77, no. 3, pp. 1045-1053, April 1985.

[5] A.M. Stankovic, B.C. Lesieutre, and T. Aydin, "Modeling and Analysis of Single-Phase Induction Machines with Dynamic Phasors," *IEEE Transactions on Power Systems,* vol. 14, no.1, pp. 9-14, Feb. 1999.

[6] P.C. Sen, *Principles of Electric Machines and Power Electronics, Second Edition,* John Wiley & Sons, Inc., 1997.

[7] T. Demiray, F. Milano, and G. Andersson, "Dynamic Phasor Modeling of the Doubly-fed Induction Generator under Unbalanced Conditions," *Power Tech, 2007 IEEE Lausanne*, pp. 1049-1054, 1-5 July 2007.

[8] P.C. Krause Oleg, Wasynczuk, and Scott D. Sudhoff. *Analysis of Electric Machinery and Drive Systems*, Second Edition, Wiley-Interscience, 2002.

[9] G.C. Verghese, I.J. Perez-Arria, and F.C. Schweppe, "Selective Modal Analysis with Applications to Electric Power Systems, Parts I and II," *IEEE Transactions on Power Apparatus and Systems*, vol. PAS-101, Sept. 1982, 3117-3134.

[10] P.C. Krause, O. Wasynczuk and S. Sudhoff. *Analysis of Electric Machinery*, IEEE Press, 1995.

[11] J.A. Sanders and F. Verhulst. *Averaging Methods in Nonlinear Dynamical Systems*. New York: Springer-Verlag, 1985.

APPENDIX A

STANDARD AVERAGING THEORY

The theory of averaging is a technique for replacing a possibly time-varying vector field by its average over time with the goal of obtaining asymptotic approximations of the original system [11]. Consider a first-order differential equation of the form

$$\frac{dx}{dt} = \epsilon f(x,t,\epsilon), \qquad x(0) = x_o, \qquad x,\ x_o \in D \subset \mathbf{R} \tag{A.1}$$

where D is an open set on which f is defined. The parameter ϵ is assumed small. Let us also assume that f is periodic in t with period T. Let us define the average

$$\bar{f}(x) = \frac{1}{T}\int_0^T f(x,s,0)\ ds \tag{A.2}$$

The idea behind averaging is to replace the nonautonomous differential equation (1) with a first-order averaged and autonomous differential equation

$$\frac{dz}{dt} = \epsilon \bar{f}(z), \qquad z(0) = x_o \tag{A.3}$$

Let $x(t)$ be the solution of (A.1) and let $z(t)$ be the solution of (A.3) and let L, independent of ϵ, be such that $z(t) \in D$ for $0 \leq \epsilon t \leq L$. Then, there exists an ϵ-independent constant C [11] such that

$$||x(t) - z(t)|| \leq C\epsilon \tag{A.4}$$

for $0 \leq \epsilon t \leq L$. We say that

$$x(t) = z(t) + O(\epsilon) \tag{A.5}$$

on the time interval T/ϵ.

As an example, consider the equation

$$\frac{dx}{dt} = \epsilon(x(1-x) + \sin t), \qquad x(0) = 2, \ \epsilon = 0.05 \tag{A.6}$$

which models a slow logistic growth (the $x(1-x)$ term) with a seasonal influence (the $\sin t$ term). Its averaged system is

$$\frac{dz}{dt} = \epsilon(z(1-z)), \qquad z(0) = 2, \ \epsilon = 0.05 \tag{A.7}$$

Figure A.1 shows the exact solution in a solid line and its averaged approximation in a dashed line showing that the seasonal influence is $O(\epsilon)$.

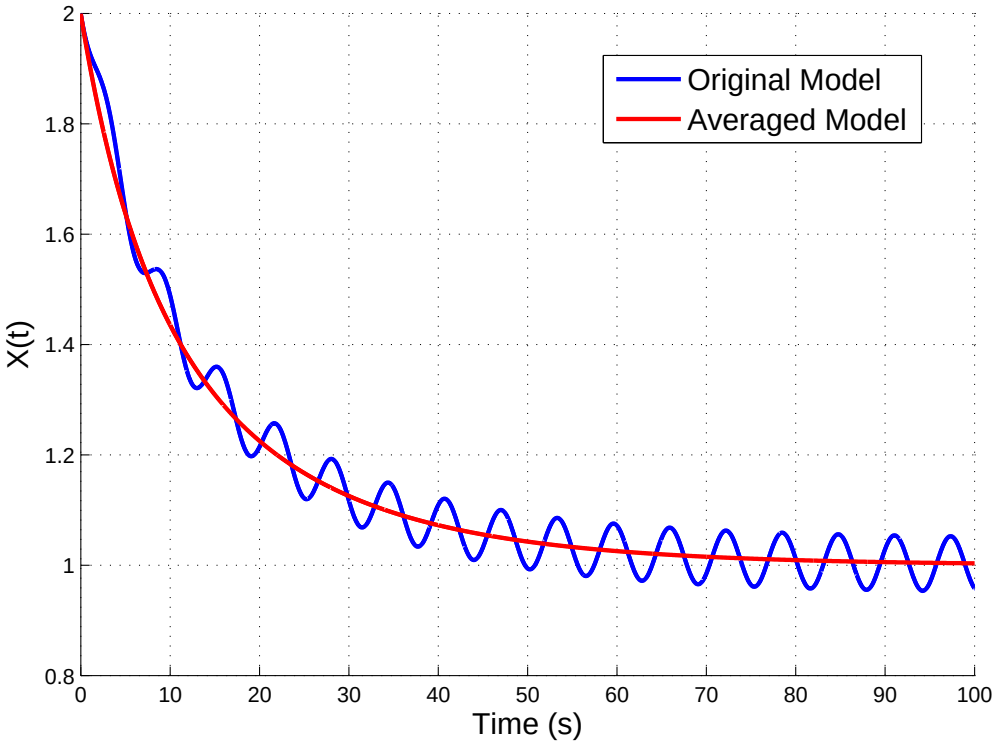

Figure A.1: Solutions of the Original and Averaged Differential Equations

APPENDIX B

MODELING OF A THREE-PHASE INDUCTION MACHINE

In nearly all applications, the induction machine is operated as a motor with the stator windings connected to a balanced three-phase source and the rotor windings short-circuited. The flux-current relationships of a three-phase induction machine with sinusoidally-distributed windings are given in [8] (page 140) as

$$\begin{bmatrix} \lambda_{sa} \\ \lambda_{sb} \\ \lambda_{sc} \\ \lambda_{ra} \\ \lambda_{rb} \\ \lambda_{rc} \end{bmatrix} = \begin{bmatrix} L_{sasa} & L_{sasb} & L_{sasc} & L_{sara} & L_{sarb} & L_{sarc} \\ L_{sbsa} & L_{sbsb} & L_{sbsc} & L_{sbra} & L_{sbrb} & L_{sbrc} \\ L_{scsa} & L_{scsb} & L_{scsc} & L_{scra} & L_{scrb} & L_{scrc} \\ L_{rasa} & L_{rasb} & L_{rasc} & L_{rara} & L_{rarb} & L_{rarc} \\ L_{rbsa} & L_{rbsb} & L_{rbsc} & L_{rbra} & L_{rbrb} & L_{rbrc} \\ L_{rcsa} & L_{rcsb} & L_{rcsc} & L_{rcra} & L_{rcrb} & L_{rcrc} \end{bmatrix} \begin{bmatrix} i_{sa} \\ i_{sb} \\ i_{sc} \\ i_{ra} \\ i_{rb} \\ i_{rc} \end{bmatrix} \tag{B.1}$$

where

$$L_{sasa} = L_{sbsb} = L_{scsc} = L_{\ell s} + L_{ms} \tag{B.2}$$

$$L_{sasb} = L_{sbsa} = L_{sasc} = L_{scsa} = L_{sbsc} = L_{scsb} = -\frac{L_{ms}}{2} \tag{B.3}$$

$$L_{rarb} = L_{rarc} = L_{rbra} = L_{rbrc} = L_{rcra} = L_{rcrb} = -\frac{L_{ms}}{2} \tag{B.4}$$

$$L_{sara} = L_{sbrb} = L_{scrc} = L_{ms}\cos\theta \tag{B.5}$$

$$L_{sarb} = L_{sbrc} = L_{scra} = L_{rasc} = L_{rbsa} = L_{rcsb} = L_{ms}\cos(\theta + 120^o) \quad \text{(B.6)}$$

$$L_{sarc} = L_{sbra} = L_{scrb} = L_{rasb} = L_{rbsc} = L_{rcsa} = L_{ms}\cos(\theta - 120^o) \quad \text{(B.7)}$$

$$L_{rara} = L_{rbrb} = L_{rcrc} = L_{\ell r} + L_{ms} \quad \text{(B.8)}$$

assuming that rotor variables have been referred to the stator side. By defining the following stator and rotor space vectors of currents and fluxes

$$\vec{\lambda}_s = \frac{2}{3}\left[\lambda_{sa} + \bar{a}\lambda_{sb} + \bar{a}^2\lambda_{sc}\right] \quad \text{(B.9)}$$

$$\vec{i}_s = \frac{2}{3}[i_{sa} + \bar{a}i_{rb} + \bar{a}^2 i_{rc}] \quad \text{(B.10)}$$

$$\vec{\lambda}_r = \frac{2}{3}\left[\lambda_{ra} + \bar{a}\lambda_{rb} + \bar{a}^2\lambda_{rc}\right] \quad \text{(B.11)}$$

$$\vec{i}_r = \frac{2}{3}[i_{ra} + \bar{a}i_{rb} + \bar{a}^2 i_{rc}] \quad \text{(B.12)}$$

where $\bar{a} = 1\angle 120^o$, the flux-current relationships of a three-phase induction machine can be compactly expressed as

$$\vec{\lambda}_s = (L_{\ell s} + \frac{3}{2}L_{ms})\vec{i}_s + \frac{3}{2}L_{ms}\vec{i}_r e^{j\theta} \quad \text{(B.13)}$$

$$\vec{\lambda}_r = \frac{3}{2}L_{ms}\vec{i}_s e^{-j\theta} + (L_{\ell r} + \frac{3}{2}L_{ms})\vec{i}_r. \quad \text{(B.14)}$$

The voltage equations for both stator and rotor windings are defined as follows

$$v_{sa} = R_s i_{sa} + \frac{d\lambda_{sa}}{dt} \quad \text{(B.15)}$$

$$v_{sb} = R_s i_{sb} + \frac{d\lambda_{sb}}{dt} \quad \text{(B.16)}$$

$$v_{sc} = R_s i_{sc} + \frac{d\lambda_{sc}}{dt} \quad \text{(B.17)}$$

$$0 = R_s i_{sa} + \frac{d\lambda_{sa}}{dt} \tag{B.18}$$

$$0 = R_s i_{sb} + \frac{d\lambda_{sb}}{dt} \tag{B.19}$$

$$0 = R_s i_{sc} + \frac{d\lambda_{sc}}{dt} \tag{B.20}$$

and, in vector form

$$\vec{v}_s = R_s \vec{i}_s + \frac{d\vec{\lambda}_s}{dt} \tag{B.21}$$

$$0 = R_r \vec{i}_r + \frac{d\vec{\lambda}_r}{dt} \tag{B.22}$$

where $\vec{\lambda}_s$ and $\vec{\lambda}_r$ are given by Equations (B.13) and (B.14).

B.1 Torque Equation in a Three-Phase Induction Machine

Assuming an electrically-linear machine, the magnetic co-energy is given by

$$W'_m = \frac{1}{2}\lambda_{sa} i_{ra} + \frac{1}{2}\lambda_{sb} i_{sb} + \frac{1}{2}\lambda_{sc} i_{sc} + \frac{1}{2}\lambda_{ra} i_{ra} + \frac{1}{2}\lambda_{rb} i_{rb} + \frac{1}{2}\lambda_{rc} i_{rc}. \tag{B.23}$$

Using the previously-defined space vectors, it can be shown that

$$\begin{aligned} \vec{\lambda}_s \vec{i}_s^{\,*} &= \frac{2}{3}(\lambda_{sa} i_{sa} + \lambda_{sb} i_{sb} + \lambda_{sc} i_{sc}) - \frac{2}{9} L_{\ell s} (i_{sa} + i_{sb} + i_{sc})^2 \\ &+ j\frac{2\sqrt{3}}{9}\left[\lambda_{sa}(i_{sc} - i_{sb}) + \lambda_{sb}(i_{sa} - i_{sc}) + \lambda_{sc}(i_{sb} - i_{sa})\right]. \end{aligned} \tag{B.24}$$

Hence,

$$(\lambda_{sa} i_{sa} + \lambda_{sb} i_{sb} + \lambda_{sc} i_{sc}) = \frac{3}{2}\Re_e\{\vec{\lambda}_s \vec{i}_s^{\,*}\} + \frac{1}{3} L_{\ell s} (i_{sa} + i_{sb} + i_{sc})^2 \tag{B.25}$$

Similarly, for the rotor windings, it can be shown that

$$(\lambda_{ra}i_{ra} + \lambda_{rb}i_{rb} + \lambda_{rc}i_{rc}) = \frac{3}{2}\Re_e\{\vec{\lambda}_r\vec{i}_r^*\} + \frac{1}{3}L_{\ell r}(i_{ra} + i_{rb} + i_{rc})^2. \quad \text{(B.26)}$$

Using Equations (B.25) and (B.26), the co-energy can be expressed as

$$\begin{aligned}
W'_m &= \frac{1}{2}\lambda_{sa}i_{ra} + \frac{1}{2}\lambda_{sb}i_{sb} + \frac{1}{2}\lambda_{sc}i_{sc} + \frac{1}{2}\lambda_{ra}i_{ra} + \frac{1}{2}\lambda_{rb}i_{rb} + \frac{1}{2}\lambda_{rc}i_{rc} && \text{(B.27)}\\
&= \frac{1}{2}\left(\lambda_{sa}i_{sa} + \lambda_{sb}i_{sb} + \lambda_{sc}i_{sc}\right) + \frac{1}{2}\left(\lambda_{ra}i_{ra} + \lambda_{rb}i_{rb} + \lambda_{rc}i_{rc}\right) && \text{(B.28)}\\
&= \frac{1}{2}\left(\frac{3}{2}\Re_e\{\vec{\lambda}_s\vec{i}_s^*\} + \frac{1}{3}L_{\ell r}(i_{sa} + i_{sb} + i_{sc})^2\right)\\
&\quad + \frac{1}{2}\left(\frac{3}{2}\Re_e\{\vec{\lambda}_r\vec{i}_r^*\} + \frac{1}{3}L_{\ell r}(i_{ra} + i_{rb} + i_{rc})^2\right) && \text{(B.29)}\\
&= \frac{3}{4}\Re_e\{\vec{\lambda}_s\vec{i}_s^* + \vec{\lambda}_r\vec{i}_r^*\} + \frac{1}{6}L_{\ell r}(i_{sa} + i_{sb} + i_{sc})^2\\
&\quad + \frac{1}{6}L_{\ell r}(i_{ra} + i_{rb} + i_{rc})^2 && \text{(B.30)}
\end{aligned}$$

Taking the electromagnetic co-energy as a function of the stator and rotor currents and the electrical angle θ,

$$W'_m = W'_m(i_{sa}, i_{sb}, i_{sc}, i_{ra}, i_{rb}, i_{rc}, \theta) \quad \text{(B.31)}$$

the electromagnetic torque is obtained as the partial derivative of the co-energy with respect to the physical angle of rotation θ_m

$$T_e = \frac{\partial W'_m}{\partial \theta_m} = \left(\frac{p}{2}\right)\frac{\partial W'_m}{\partial \theta} \quad \text{(B.32)}$$

since

$$\theta_m = \left(\frac{2}{p}\right)\theta. \tag{B.33}$$

Thus,

$$T_e = \left(\frac{p}{2}\right)\frac{\partial}{\partial\theta}\left[\frac{3}{4}(\Re e\{\vec{\lambda}_s\vec{i}_s^* + \vec{\lambda}_r\vec{i}_r^*\}) + \frac{L_{\ell r}}{6}\left((i_{sa}+i_{sb}+i_{sc})^2 + (i_{ra}+i_{rb}+i_{rc})^2\right)\right]$$

which simplifies to

$$T_e = \left(\frac{3}{4}\right)\left(\frac{p}{2}\right)\frac{\partial}{\partial\theta}\left(\Re e\{\vec{\lambda}_s\vec{i}_s^* + \vec{\lambda}_r\vec{i}_r^*\}\right) \tag{B.34}$$

Using the flux-current relationships from Equation (B.13) and (B.14), we have

$$\begin{aligned} T_e = \left(\frac{3}{4}\right)\left(\frac{p}{2}\right)\frac{\partial}{\partial\theta}\Bigg[\Re e\Bigg\{&(L_{\ell s}+\frac{3}{2}L_{ms})\vec{i}_s\vec{i}_s^* + \frac{3}{2}L_{ms}\vec{i}_r e^{j\theta}\vec{i}_s^* + \frac{3}{2}L_{ms}e^{-j\theta}\vec{i}_s\vec{i}_r^* \\ &+(L_{\ell r}+\frac{3}{2}L_{ms})\vec{i}_r\vec{i}_r^*\Bigg\}\Bigg]. \end{aligned} \tag{B.35}$$

Hence,

$$T_e = \left(\frac{3}{4}\right)\left(\frac{p}{2}\right)\frac{\partial}{\partial\theta}\left[\Re e\left\{\frac{3}{2}L_{ms}\vec{i}_r e^{j\theta}\vec{i}_s^* + \frac{3}{2}L_{ms}e^{-j\theta}\vec{i}_s\vec{i}_r^*\right\}\right] \tag{B.36}$$

or

$$T_e = \left(\frac{3}{4}\right)\left(\frac{p}{2}\right)\left[\Re e\left\{j\frac{3}{2}L_{ms}\vec{i}_r e^{j\theta}\vec{i}_s^* - j\frac{3}{2}L_{ms}e^{-j\theta}\vec{i}_s\vec{i}_r^*\right\}\right]. \tag{B.37}$$

After simplifying the above expression, the developed electromagnetic torque is

$$T_e = \left(\frac{3}{2}\right)\left(\frac{p}{2}\right)\left(\frac{3}{2}L_{ms}\right)\Im m\left(\vec{i}_s\vec{i}_r^* e^{-j\theta}\right). \tag{B.38}$$